PERFORM
WP3. Results of laboratory testing and on-site monitoring of corrosion in geothermal water

Deliverable D4

Prepared by: FT:
Johan Braüner Nielsen
Troels Mathiesen

Checked by: GFZ: Simona Regenspurg

Approved by: GFZ: Simona Regenspurg

PERFORM is one of nine projects under the GEOTHERMICA – ERA NET The overarching target of PERFORM is to improve geothermal system performance, lower operational expenses and extend the life-time of infrastructure by the concept of combining data collection, predictive modelling, innovative technology development and in-situ validation. The improvement of geothermal plant performance from the proposed work is expected to result in an increase of the energy output by 10 to 50%. In order to reach this goal PERFORM will establish a single and shared knowledge database, build predictive models and demonstrate new and improved, cost-effective technologies which will reduce or even eliminate flow-obstructive scaling, clogging, and resistance to fluid (re-)injection at eight geothermal plants across Europe.

The GEOTHERMICA is supported by the European Union's HORIZON 2020 programme for research, technological development and demonstration under grant agreement No 731117

About PERFORM

Despite years of experience with geothermal systems, the geothermal sector still faces a significant number of underperforming doublets, posing a strong limitation on a region's growth of geothermal energy utilization. A key operational challenge in geothermal energy production is restricted flow. Major obstacles for geothermal flow are scaling (mineral deposition), clogging (solid micro-particle deposition), corrosion and inefficient injection strategies. These issues result in high and mostly unforeseen costs for workovers, and additionally reduce production. In order to overcome these challenges, the consolidation and sharing of knowledge, including validated strategies for prevention and mitigation needs to be in place.

Therefore a consortium consisting of De Nationale Geologiske Undersøgelser for Danmark og Grønland (GEUS) and FORCE Technology from Denmark, Helmholtz Centre Potsdam German Research Centre for Geosciences (GFZ) and Hydroisotop GmbH from Germany and Ammerlaan Geothermie B.V., Greenwell Westland B.V., Wageningen Food & Biobased Research and ECN part of TNO from the Netherlands proposed a GEOTHERMICA project PERFORM, which has been granted. The overarching target of PERFORM is to improve geothermal system performance, lower operational expenses and extend the life-time of infrastructure by the concept of combining data collection, predictive modelling, innovative technology development and in-situ validation. The improvement of geothermal plant performance from the proposed work is expected to result in an increase of the energy output by 10 to 50%. In order to reach this goal PERFORM will establish a single and shared knowledge database, build predictive models and demonstrate new and improved, cost-effective technologies which will reduce or even eliminate flow-obstructive scaling, clogging, and resistance to fluid (re-)injection at eight geothermal plants across Europe.

Based on experiences from operating geothermal sites within the EU, PERFORM will establish a single knowledge database containing information on operational, chemical and physical aspects of geothermal energy production. The database enables sharing experiences from operating geothermal doublets located in various countries and comparing the performance of the different geothermal reservoirs.
PERFORM builds predictive models that allow for pinpointing the most likely sources and causes of failure, as well as the best options for injectivity improvement. The integrated models will provide forecasting for scaling, productivity, and injectivity on short- and long- time scales, supporting early warning and planning of mitigation measures. Coupled thermo-hydro-mechanical-chemical simulators will allow for evaluation of injection temperature that apart for increasing flow will also increase the energy output.

Data and knowledge gathering and technology demonstration is planned for eight geothermal plants across Europe. Demonstration of new and improved, cost-effective technologies will allow for the reduction or even elimination of flow-obstructive scaling, clogging, and resistance to fluid (re-)injection. The technologies include low-cost cation extraction filters, self-cleaning particle removal appliances, H_2S removal technology and soft-stimulating injection procedures (thermal and CO_2-injection). The goal is to provide a set of new and improved, low-cost and environmentally friendly technology alternatives. PERFORM integrates the knowledge database, predictive modelling and advanced technologies into a design and operation toolbox, which will be tied to economical calculations. The toolbox will enable stakeholders and specifically geothermal operators to plan future operations, mitigate existing obstructions, and optimize production/injection procedures, thus ensuring maximum energy production when needed.

This project has been subsidized through the ERANET Cofund GEOTHERMICA (Project no. 731117), from the European Commission, Topsector Energy subsidy from the Ministry of Economic Affairs of the Netherlands, Federal Ministry for Economic Affairs and Energy of Germany and EUDP.

Summary

Despite years of experience with geothermal systems, the geothermal sector still faces a significant number of challenges. Among these are deposition of solids and corrosion of various section of the systems. The efforts on understanding corrosion in geothermal waters take basis from the shared knowledge of GFZ, TNO, GEUS and FORCE Technology.

This report treats data obtained from on-site monitoring obtained in PERFORM in extension to the Danish project data. FORCE Technology's involvement in monitoring three Danish geothermal plants has indicated lead deposition and oxygen ingress as the main causes for the corrosion challenges in the plants. In addition, experience from the Netherlands also point to lead as a reason for corrosion, as well as corrosion due to CO_2.

Parametric laboratory testing has been carried out to investigate the effect of lead in solution and its deposition on the steel in artificial Margretheholm brine solution, with varying concentrations of lead in solution (0.0, 3.0 and 22.5 mg/l Pb(II)) added as lead chloride ($PbCl_2$). This has been done using electrochemical techniques i.e., LPR, OCP, potentiodynamic polarisation and zero resistance amperometry (ZRA) on a galvanic coupling between steel and steel with lead in the brine solution. Also the effect of oxygen ingress on corrosion resistant alloys (CRA) has been investigated using some of the same techniques. This also applies for the corrosion contribution due to galvanic effect when coupling CRA and carbon steel in CO_2 containing brine.

These studies showed that lead is more noble than steel with and without lead in solution, thus explaining the galvanic dissolution of steel. It also showed that while the temperature (25 and 70 °C) has no significant effect on the corrosion rate of carbon steel in lead-free brine it had a large effect with 22.5 mg/l Pb(II) in solution. The low concentration with 3.0 mg/l showed no effect at 25 °C and a deviating reduction in corrosion rate at 70 °C.

Estimated corrosion rates based on Evans diagrams, showed increasing corrosion rate of carbon steel with increasing lead concentration and the highest corrosion rate with metallic lead as cathode in Pb(II) containing brine. Thus, indicating the ongoing process in the geothermal pipe systems with lead depositions and lead in solution leading to high corrosion rates of the adjacent carbon steel. Custom build double-cell zero resistance amperometry investigating the galvanic effect of a coupling between carbon steel and carbon steel with deposition of lead from solution showed great influence of temperature, as measured current greatly increased from 25 to 70 °C.

Due to use in the Margretheholm plant, the effect of corrosion inhibitor (Nalco GEO942) was also investigated. Investigation showed that the dosage of corrosion inhibitor has only limited effect (2-5 times reduction in corrosion rate). Linear polarisation resistance measurements showed that the efficacy of the inhibitor increased with time, likely due to more time to adsorb to the surface or consumption of the lead in solution. Interestingly efficacy declined in a system without Pb(II) with increase in inhibitor from 1 to 10 ml/l at 70 °C. This is possibly explained by the increase in potential by adding the inhibitor.

Investigation into the effect of oxygen ingress on the corrosion performance of AISI 316L did not show a significant difference in open circuit potential or pitting potential with increasing amount of dissolved oxygen, because the alloy show bordline corrosion in the geothermal. When observing the increase of the platinum ORP we find that the tolerance to oxygen ingress is extremely small for AISI 316L.

Studying the effect of CO_2 on the coupling of carbon steel and CRAs (AISI 316L), reveals the presence of CO_2 will allow the stainless steel to function as a cathode in the coupling with carbon steel leading to a small increase in corrosion of the latter due to galvanic corrosion.

Table of Content

About PERFORM **3**
Summary **4**
1 Introduction **6**
2 Results of on-site visits and monitoring **7**
1.1 On-site monitoring and water sampling 8
1.2 Water sampling in Thisted 2019 8
3 Parametric laboratory testing **11**
1.3 Effect of temperature on metallic lead and carbon steel 11
1.4 Lead deposition 14
1.4.1 Tafel extrapolation 14
1.4.2 Evans diagrams 16
1.4.3 Zero resistance amperometry 18
1.4.4 Corrosion inhibitor 22
1.4.5 Calculations on galvanic element from lead deposition 26
1.5 Corrosion resistant alloys 28
1.5.1 Effect of lead in solution 28
1.5.2 Effect of oxygen ingress 32
1.6 Galvanic effect of CO_2 35
4 Discussion and conclusions **38**
5 References and literature **43**
Appendix **44**

1 Introduction

The efforts on understanding corrosion in geothermal waters take basis in the shared knowledge GFZ, TNO, GEUS and FORCE Technology. GFZ has dealt with corrosion issues of steel due to copper and lead deposition for many years. TNO have studied similar corrosion issues (esp. lead) in the Netherlands, but corrosion due to CO_2 corrosion is also observed in some plants. The recent activities at FORCE Technology have together with GEUS involved monitoring in three Danish geothermal plants, indicating lead deposition and air ingress as the main corrosion challenges in the plants.

On this basis, a series of tests have been performed to support the understanding of corrosion and to establish mitigating actions. It was originally planned to perform corrosion monitoring at the three Danish sites. However, due to unexpected operational issues and shutdowns in Margretheholm and in Sønderborg, the on-site monitoring has been limited to Thisted. This circumstance has given us more room for corrosion testing in the laboratory.

As stated in the project application, the corrosion studies aim at preventing CO_2 and electrochemical corrosion and investigate the use of corrosion resistant alloys (CRAs). Within this scope and based on the current problems in the Danish and German plants, the tests have mainly focused on studying the items listed below.

- Monitor changes in dissolved oxygen and pH during operation of geothermal plants
- Study effects of lead and copper deposition on corrosion of steel, including effects of temperature and corrosion inhibitors
- Study effects of lead and copper deposition on corrosion behaviour or CRAs
- Calculate extension of galvanic element by lead as function of chloride/conductivity.
- Study effect of dissolved oxygen on corrosion resistance of CRAs
- Study influence of CO_2 on galvanic corrosion

The above testing is mostly based on parametric studies conducted in the laboratory. As a basis low alloyed steel (St 37 or St 52) and pure lead have been used for studying galvanic corrosion under anoxic conditions. These studies include the influence of temperature and lead ion concentration in the brine at 25 °C (ambient pressure) and 70 °C (ambient and 70 bar in autoclave). The brine solution was artificial, mimicking Margretheholm conditions as this is the only Danish site with lead in the brine, and thus comparable to other European sites experiencing issues with this, e.g. Gross Schönebeck.

Multiple testing techniques were applied. Among these are customised setups for galvanically coupled steel with steel where deposition of lead takes place. Likewise, a customised setup was built to control the oxygen ingress in the ppb range while testing the corrosion resistance of CRAs. The corrosion resistant alloys (CRAs) included EN 1.4404 (AISI 316L) in all tests and Nickel Alloy 31 in fewer tests.

CO_2 is well-studied because it is a major problem in the oil & gas production. Likewise, mathematical modelling is well-established and often available for free, such as NORSOK M-506 [13]. Therefore, our approach for studying CO_2 corrosion was slightly different from that often found in the literature. Using the customised galvanic cell we wanted to see if CO_2 could induce galvanic effects between different metals (steel and CRA) in the same way as oxygen can cause differential aeration cells. This study was motivated by the fact that large surfaces of CRAs connected directly to carbon steel piping in the surface plant.

Some of the testing was conducted as part of the Master Thesis of Ms. Anastasia Stoljarova, Freie Universität Berlin, who, as a direct consequence of the collaboration between GFZ and FT in the current project, came on exchange to work at FT. This exchange programme has been fruitful for

the current project and it has resulted in a thesis report as well as an article in the recognised journal Geothermics, both supporting the work in presented in this report [1,2].

As part of the above, corrosion has been a main item for optimizing the operation and extending the lifetime of geothermal plants. This report concludes the work conducted as part of WP 3.4 'Corrosion and the effect of corrosion resistant alloys' at FORCE Technology and at GFZ. It completes delivery D4 in the project plan.

2 Results of on-site visits and monitoring

Prior to PERFORM an assessment of the Danish geothermal sites had been conducted by visiting the plants and reviewing their service history. For the sake of context some observations made during these visits are summarised below:

Margretheholm

The Margretheholm site has not been visited within the framework of PERFORM. However, known observations are dark-grey deposits in nearly all the inspected pipes. These deposits have subsequently been confirmed to be primarily constituted of metallic lead. In addition, one incident of penetrating corrosion had occurred in an elbow immediately after the heat exchanger. The leak was presumed to have been caused by internal corrosion caused by lead deposits in conjunction with turbulent flow. This mechanism has previously been described by Schröder [3]. A report by GEUS in 2015 also suggests this mechanism [4-7].

Sønderborg

The geothermal plant in Sønderborg was visited several times in 2016, 2017 and 2018. Upon inspection, no corrosion was observed except from what appeared to be superficial internal rust on some of the pipes leading to the injection well. Inspection of excess tubing similar to that used in the plant revealed significant amounts of rust flakes inside the tubing. It is presumed this come from mill scale as the tubing was still sealed with plastic end caps.

The presence and release of mill scale may be an explanation for the injection issues experienced at this site, as it may clog up the sieve at the injection well. Being difficult to dissolve it is likely that an ordinary acid job on the well may not be sufficient to remove it [8].

Indication of oxygen ingress was seen with the depletion of carbon steel anodes found in the AISI 316 filter housing after roughly six months. Such a consumption rate indicates oxygen ingress beyond that from replacement of filters alone. Corrosion monitoring performed in years 2017-2018 also support this assessment [8].

Thisted

The Thisted plant has been running without issues for 35 years. A section from a decommissioned pipe with more than 30 years of service was available for inspection as result of the latest injection well commissioning. The decommissioned pipe section revealed no discernible reduction in wall thickness with merely light superficial corrosion, likely caused by water remnants on the surface after sectioning the pipe. To a large degree, the new injection well has been equipped with composite tubing to mitigate corrosion issues and save weight.

1.1 On-site monitoring and water sampling

Ongoing corrosion monitoring by FT in Danish geothermal plants has been challenging due to operational issues and shutdowns of these plants. From the Margretheholm site, oxygen reduction potential (ORP), corrosion rate (using linear polarisation resistance, LPR) and pH was recorded back in 2017. In addition, corrosion coupons to determine corrosion type, weight loss and scaling was also exposed. Currently this is the only corrosion rate data available from this site, as the site was shut down later the same year and has remained closed since then. Therefore, no additional data were collected from this site, despite this having been intended at the proposal of this project.

Measuring rigs for monitoring the environmental changes were installed at the production well and injection well in the Sønderborg site in December 2018. This includes measurement of dissolved oxygen (DO), pH and oxygen-reduction potential (ORP). Additionally, the rig previously used for corrosion rate measurements in 2017/2018 was installed at the injection well. However, due to unforeseen issues with injectivity, the plant was shut down after just two weeks of operation in December 2018. Only one week of data monitoring from the production well was possible. However, the corrosion data from 2017/2018 are available for the PERFORM project. It is considered unlikely that additional data from this site can be collected within this project duration. As the Sønderborg plant was shut down in December 2018, one measuring rig was sent to the Thisted site to be installed there. The rig was running in April 2019 measuring the same parameters as in Sønderborg. Originally, it was not intended to do any measurements in Thisted as this site has not experienced any corrosion related issues. However, the installation gives data and insight into possible issues in relation to shutdown procedures in an otherwise well-functioning plant.

1.2 Water sampling in Thisted 2019

As the Thisted plant has not experienced any corrosion issues in its service life it was originally not part of the measuring campaign. However, the long-term shutdowns of Margretheholm and Sønderborg meant the availability of a test rack and need for data. Thus, a test rack was installed near the old injection well on 26 March 2019, Figure 1. Data was recorded for roughly one month before the planned shut down for the summer season on 25 April 2019.

The setup was to measure ORP/pH and DO for a 5-minute period every 3rd hour. Some difficulties in obtaining stable readings were seen for the initial measurements, Figure 2 and 3. This may have been caused by entrapment of gasses in the respective measuring cells. This is supported by previous detection of N_2 and CH_4 gas in the brine from the production well [9]. In addition to the issues with gas entrapments was also difficulty controlling the flow, likely due to the relatively low inlet pressure. The flow control, including the control valve, should be reconsidered.

Constant flow through the cells was established leading to better readings, Figure 2 and 3. For this measuring period could the following be observed:

- Dissolved oxygen (DO) is below the detection limit, i.e. in the ppb range.
- pH is very stable at 6.2.
- Oxidation reduction potential (ORP) is -80 mV vs Ag/AgCl.

The above listed conditions are ideal to manage corrosion of the steel tubing. That the observed conditions are great for mitigating corrosion correlates well with the observed condition of the decommissioned tubing.

Especially in the case of the DO measurements, limitations in design of the water sampling rack lead to fluctuations. To improve the readings refinements, such as the addition of a degasser, may be made. In addition, a better data acquisition system that is in sync with the sampling periods is necessary, e.g. sampling only when water flows through the cells. Until then, the water sampler will require frequent supervision.

Figure 1. Automated water sampler installed near the old injection well. It measures dissolved oxygen, pH and ORP in the water after cooling and depressurising.

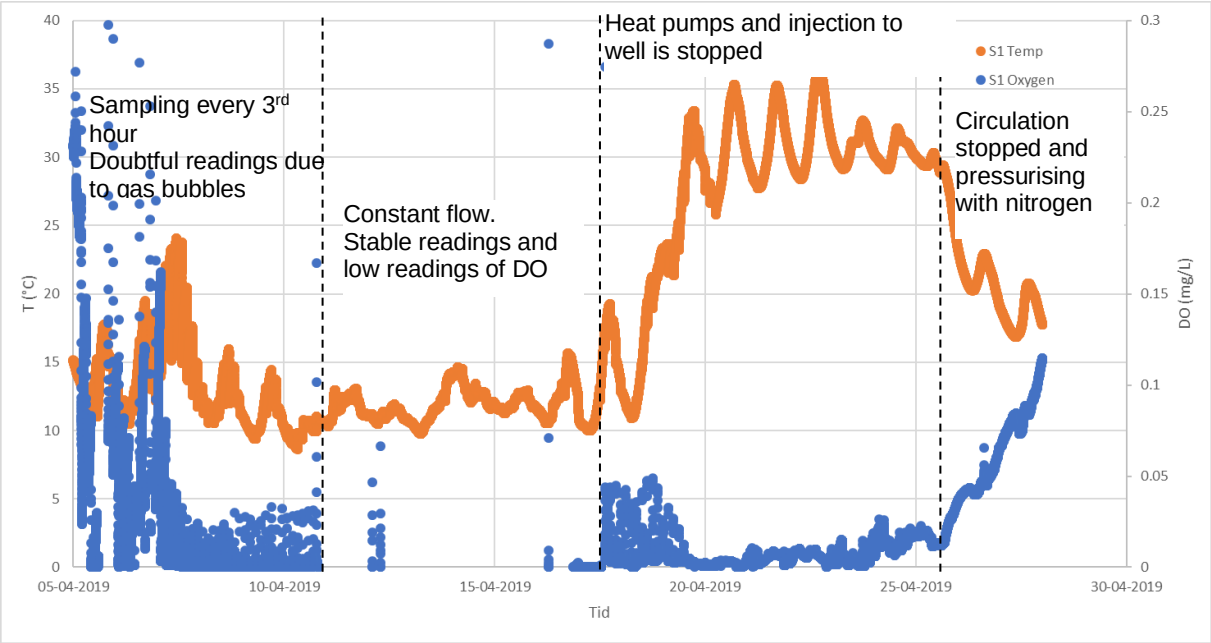

Figure 2. Result of dissolved oxygen measurements in Thisted. The temperature represents the water temperature in the measurement cell after cooling and depressurising.

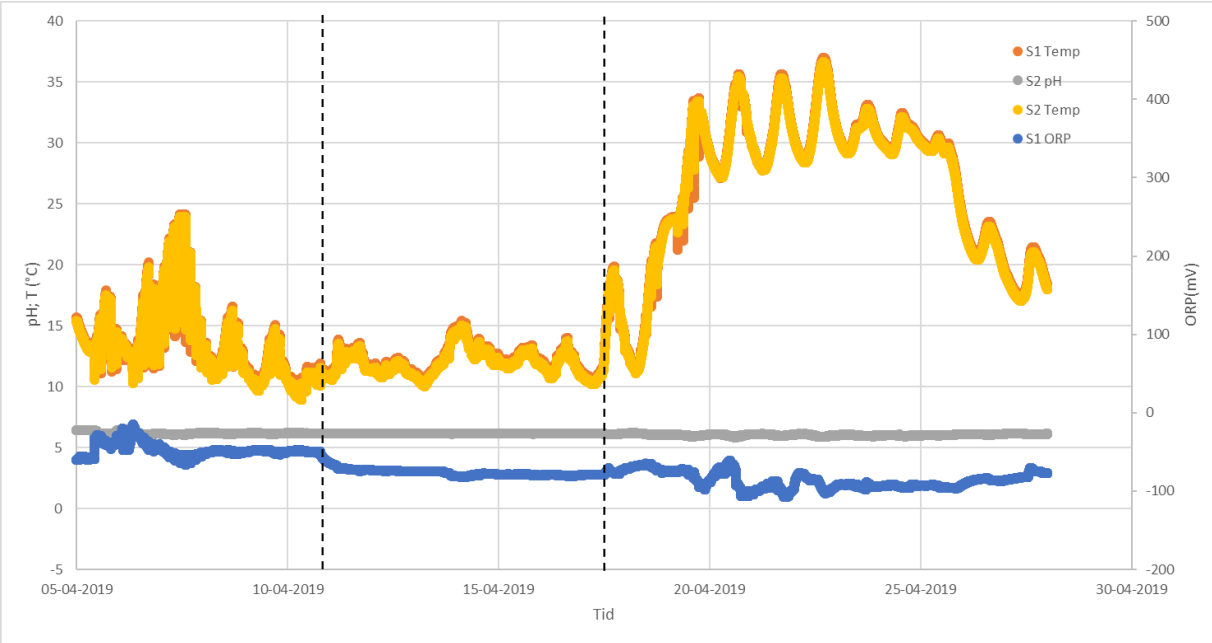

Figure 3. Result of pH and ORP measurements in Thisted. The temperature represents the water temperature in the measurement cells after cooling and depressurising.

3 Parametric laboratory testing

Effects of basic parameters affecting corrosion have been examined in the laboratory at FORCE Technology using electrochemical techniques.

1.3 Effect of temperature on metallic lead and carbon steel

Testing strictly dealing with the effect of temperature was done in a traditional glassware setup. Testing was carried out in artificial Margretheholm brine solution, with the composition listed in Table 3.1, as this is the only Danish site with lead in the brine and thus comparable to other European sites experiencing issues with this, e.g. Groß Schönebeck.

Table 3.1. Chemical composition of the artificial Margretheholm brine

Chemical compound	Mol	Molar mass	g/l
NaCl	2,2970	58,443	134,244
CaCl2.2H2O	0,5540	147,02	81,4491
MgCl2.6H2O	0,1160	203,303	23,5831
K2SO4	0,003	174,26	0,54

The tests were performed under anaerobic conditions mimicking the ideally oxygen free environment in the geothermal plants. The corrosion properties were investigated using open circuit potential (OCP), linear polarisation resistance (LPR) and potentiodynamic polarisation. The influence of temperature on corrosion properties were investigated at 25 and 70 °C as these are common operating temperatures from wellhead to the injection well in Margretheholm. Carbon steel and metallic lead test specimens were used. Pure lead was tested to obtain information about the corrosion behaviour of a metallic lead coating formed in the geothermal plant during service.

OCP measurements depicted in Figure 4 shows that lead is significantly more noble, i.e., the corrosion potential is higher, than the low alloyed carbon steel (St52/St37) in the geothermal brine. For carbon steel the effect of temperature on the OCP is negligible while temperature appear to lower the OCP for lead with increased temperature.

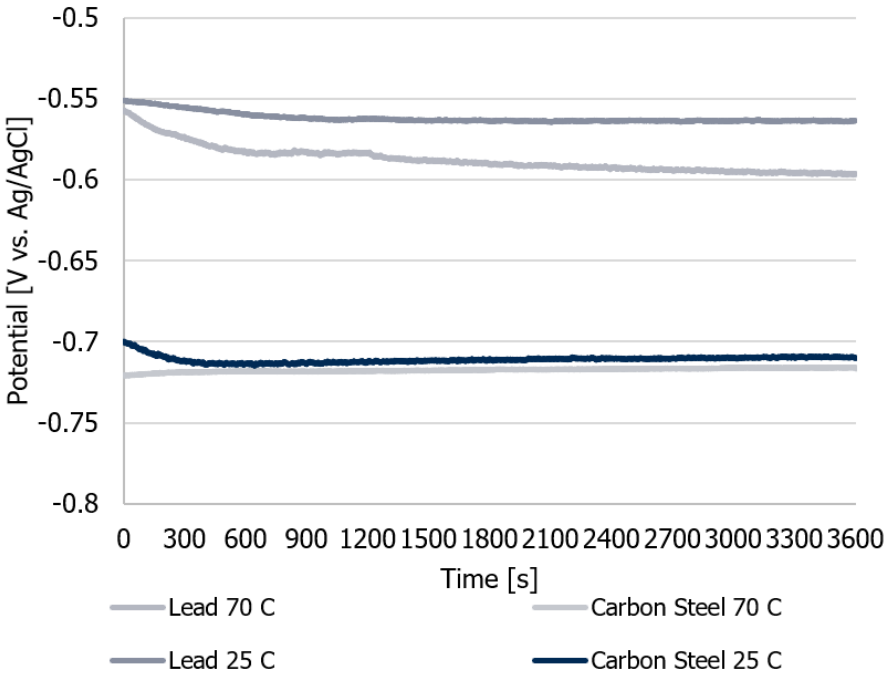

Figure 4. Open circuit potential for lead and carbon steel (St52/St37) at 25 and 70 °C. In artificial brine, deaerated with nitrogen.

That the lead is behaving more noble in the brine, is further supported by the potentiodynamic polarisation and the following Tafel fit, in order to determine corrosion potential and corrosion rate of metallic lead and carbon steel under same conditions. The polarisation curves show in Figure 5 and 6 also show only minor differences with temperature for carbon steel and lead in respect to behavior, sustained current densities and corrosion rate calculated from the Tafel fit. Both materials show active corrosion in the anodic area, although lead indicates a tendency to passivate at higher potentials than -0.45 V vs Ag/AgCl, thus beyond what has been tested in this study. The effect is especially pronounced at 25 °C, where the current drops one decade. This shows that while lead is more electropositive (noble) than carbon steel, lead has a higher corrosion rate. Meaning it is harder to initiate the corrosion of lead but once it does it will corrode faster.

The high corrosion current of lead and accompanying corrosion rate are not explained at this point; however, kinetics may play a role as may deposition of salt of Ca and Mg on the surface and the dissolution of natural lead oxide on the surface while initially being run as cathode during the test [10].
Steel by itself corrodes faster in the artificial Margretheholm brine solution at 70 °C compared to the same at 25 °C, but with little change in corrosion potential and corrosion rate. This is seen by the slight decrease in corrosion potential and the faster increase in running current with the rise in potential.

Table 3.2. Corrosion rates calculated from Tafel fit of polarisation			
Material	Temp.	Electrolyte	Corrosion rate [mm/y]
Carbon Steel	25 °C	Brine	0.023
Carbon Steel	70 °C	Brine	0.023
Lead	25 °C	Brine	0.04
Lead	70 °C	Brine	0.04

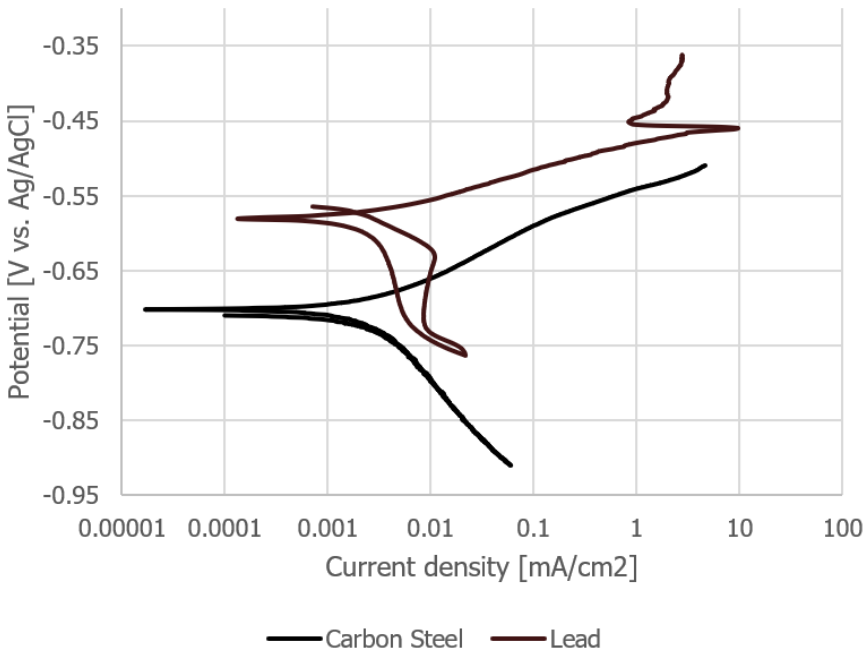

Figure 5. Potentiodynamic polarisation of carbon steel and lead in artificial brine at 25 °C. Deaerated using nitrogen.

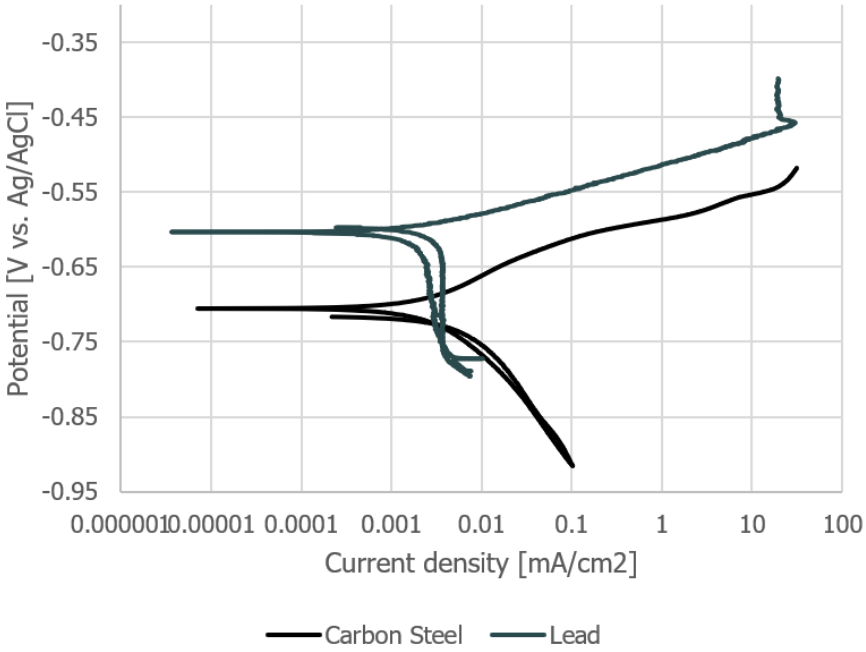

Figure 6. Potentiodynamic polarisation of carbon steel and lead in artificial brine at 70 °C. Deaerated using nitrogen.

1.4 Lead deposition

In section 3.1 it has been described how metallic lead is more noble in comparison with carbon steel, commonly utilised for tubing, thus creating a galvanic coupling leading to accelerated corrosion of the carbon steel. However, in the geothermal plant the lead will be present in solution (as Pb(II) ions) prior to deposition. The effect of lead in solution and its deposition on the steel in artificial Margretheholm brine solution has been investigated using electrochemical techniques i.e., LPR, OCP, potentiodynamic polarisation and zero resistance amperometry (ZRA) on a galvanic coupling between steel and steel with lead in the brine solution. Testing of carbon steel with lead in solution represents virgin steel tubing exposed to the brine or newly exposed areas of old tubing from under recently removed deposits and testing of metallic lead already formed deposits and their reaction in the lead containing brine. The influence of lead in solution has been investigated by the addition of 3.0 mg/l Pb(II) resembling maximum amount measured at Margretheholm water analyses and 22.5 mg/l Pb(II) corresponding to the amount applied in studies at BAM and GFZ. In both concentrations lead was added in the form of an aqueous $PbCl_2$ solution.

1.4.1 Tafel extrapolation

From the conducted potentiodynamic polarisation (Figure 7 and 8), corrosion rates have been calculated via Tafel extrapolation of the curves. From the corrosion rates, shown in Table 3.3, it is evident that the addition of a moderate concentration of lead (3.0 mg Pb(II)) to solution at low temperatures gives no significant effect while the addition of 22.5 mg Pb(II) give rise to more than a factor two increase in corrosion rate at 25 °C, and it shows almost a factor five increase from carbon steel with brine absent of Pb(II) at 70 °C. Thus, temperature appears to greatly affect the deposition rate and thus the formation of local galvanic cells increasing the corrosion of the surrounding steel. The same effect was however not seen with the addition of 3.0 mg/l Pb(II) at 70 °C, where even a reduction in corrosion rate occurred. This indicates that a single polarisation curve and Tafel extrapolation may be insufficient to describe the corrosion of the steel in conjunction with the deposition of lead and the galvanic effects this imposes.

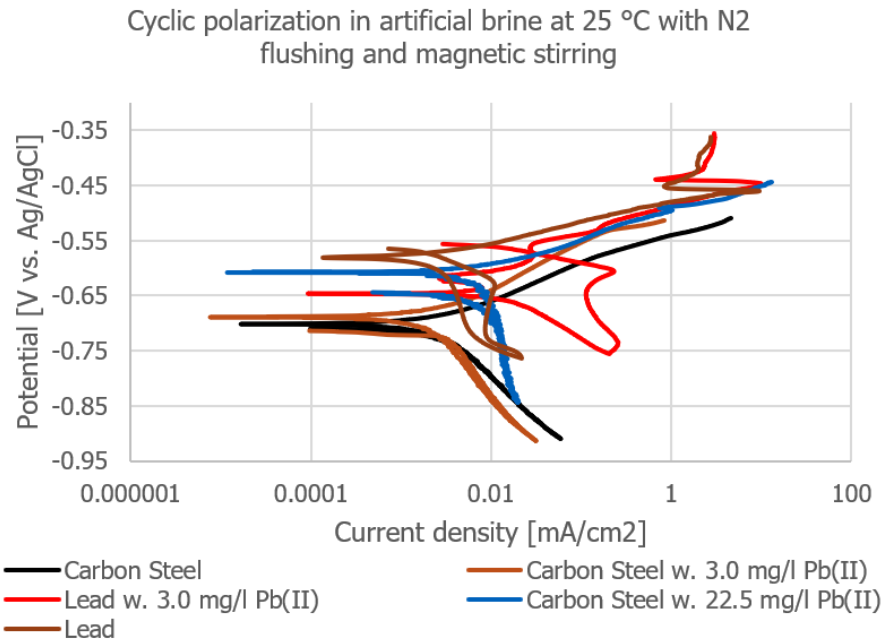

Figure 7. Cyclic polarisation in artificial brine at 25 °C with and without lead in solution. Deaerated using nitrogen.

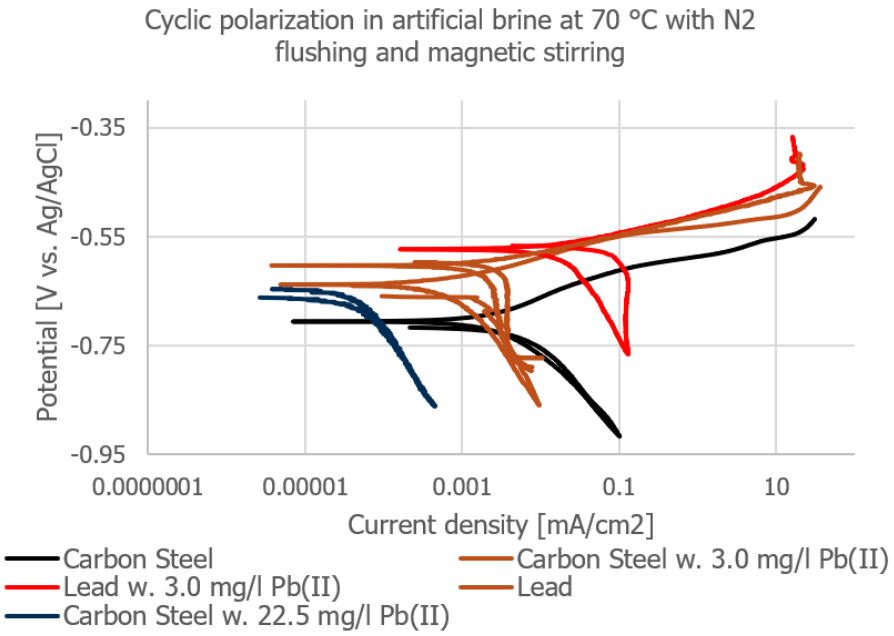

Figure 8. Cyclic polarisation in artificial brine at 25 °C with and without lead in solution. Deaerated using nitrogen.

Table 3.3. Corrosion rates calculated from Tafel fit of polarisation with lead in solution			
Material	Temp.	Electrolyte	Corrosion rate [mm/y]
Steel St52	25 °C	Brine	0.023
Steel St52	70 °C	Brine	0.023
Steel St52	25 °C	Brine + 3.0 mg/l Pb^{2+}	0.024
Steel St52	70 °C	Brine + 3.0 mg/l Pb^{2+}	0.008
Steel St52	25 °C	Brine + 22.5 mg/l Pb^{2+}	0.06
Steel St52	70 °C	Brine + 22.5 mg/l Pb^{2+}	0.11
Lead	25 °C	Brine	0.04
Lead	70 °C	Brine	0.04

1.4.2 Evans diagrams

To understand the corrosion in a system with steel, lead and with deposition of lead where galvanic coupling occurs, the corrosion rate of the least noble material (steel) is estimated using a theoretical coupling on the basis of individual polarisation curves. Figure 9 and 10 depict the results of such theoretical couplings, showing the full steel curve (anodic and cathodic) and the cathodic curves of lead (with and without lead in solution) and steel with lead in the brine, combined as Evans diagrams. Effectively, this allows the estimation of the corrosion rate of steel when positioned adjacent to any of these cathode areas in the geothermal brine (and thereby galvanically coupled). Lead with the presence of Pb(II) in solution represents a situation where sections of the tubing is already covered by deposits of lead and the continuous operation of the plant supplies brine with new lead in solution to these areas. Likewise, steel with lead in solution represents sections with virgin steel during operation. The virgin steel may be new tubing or old sections where the steel is recently exposed due to removal of deposits.

All cathodes, except steel with 3.0 mg/l Pb(II) show between a half and a full decade increase in the corrosion current (here estimated by the intersection of the lines with the anodic part of the steel curve) and thus the corrosion rate as seen from Table 3.4.

To surprise, the coupling between virgin steel and steel where deposition occurs should not increase the corrosion rate of the adjacent steel when looking at only 3.0 mg/l Pb(II). However, with the presence of 22.5 mg/l Pb(II) a significant increase is corrosion current and thus corrosion rate should occur. The calculations indicate more than a factor five increase from the virgin steel alone in the lead containing brine, while no clear effect of temperature. This indicates that lead concentration at this point is more important than the temperature. This may be due to the low concentration of lead leading to local galvanic cells on the steel sample itself when polarised with 3.0 mg/l Pb(II), whereas the 22.5 mg/l allows for a more uniform deposition thus resembling an already formed lead deposit rather than under the process of deposition.

Contradicting this, however, is the more modest increase in corrosion rate when coupling steel to metallic lead. Here is only a factor 2.5 increase at 25 °C and small factor 1.5 at 70 °C. Having metallic lead with continuous deposition of dissolved lead yields the largest increase in corrosion rate and a clear effect of temperature. In this case an increase of almost a factor 6 and a factor 16 for 25 °C and 70 °C, respectively.

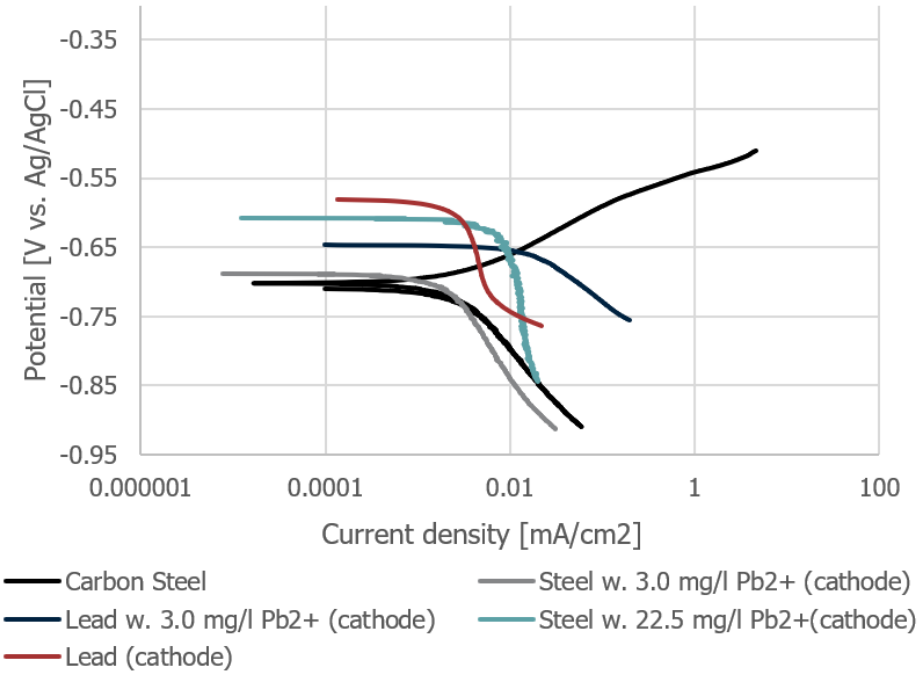

Figure 9. Anodic curve section for carbon steel plotted with cathode sections for lead and carbon steel with and without lead ions in artificial brine at 25 °C. Deaerated using nitrogen.

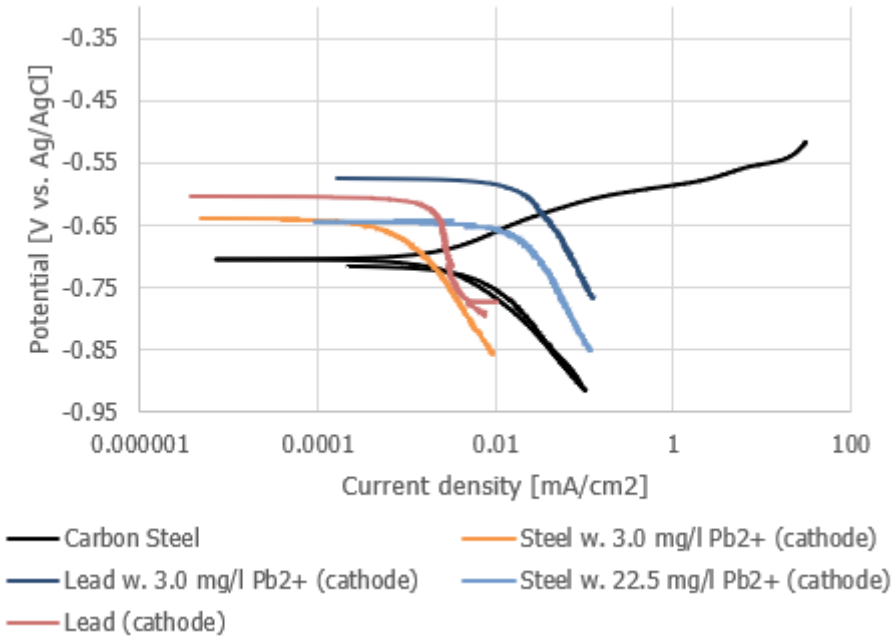

Figure 10. Anodic curve section for carbon steel plotted with cathode sections for lead and carbon steel with and without lead ions in artificial brine at 70 °C. Deaerated using nitrogen.

It appears likely that steel with only 3.0 mg/l Pb(II) at 25 °C will in fact just lead to similar corrosion rate as the positioning of the curve is only marginally different of that of the carbon steel. This minor shift can however, due to the method of approximation using the intersection of the lines, lead to the apparent decrease in corrosion rate with such a coupling. Whereas the effect of depositing lead on areas adjacent to the steel is increased if this happens where lead is already present or quickly will be with increased lead concentrations. This indicates that kinetics plays a major role as well as uniformity of the lead layer adjacent to the exposed steel.

Table 3.4. Corrosion rates calculated from theoretical coupling based on polarisation curves with lead in solution

Material	Temp.	Electrolyte	Corrosion rate [mm/y]
Steel/lead	25 °C	Brine	0.058
Steel/lead	70 °C	Brine	0.035
Steel/lead	25 °C	Brine + 3.0 mg/l Pb^{2+}	0.139
Steel/lead	70 °C	Brine + 3.0 mg/l Pb^{2+}	0.383
Steel/steel	25 °C	Brine + 3.0 mg/l Pb^{2+}	0.009
Steel/steel	70 °C	Brine + 3.0 mg/l Pb^{2+}	0.019
Steel/steel	25 °C	Brine + 22.5 mg/l Pb^{2+}	0.124
Steel/steel	70 °C	Brine + 22.5 mg/l Pb^{2+}	0.130

1.4.3 Zero resistance amperometry

To investigate how rapid the deposition of lead occurred on carbon steel and the generated current following the galvanic coupling, ZRA was performed on a coupling between carbon steel in artificial brine and carbon steel in artificial brine with 3.0 mg/l Pb(II). The ZRA measurements where initially performed by creating a salt bridge between two electrochemical cells as shown in Figure 11. This allowed for stirring and heating to be controlled exactly like done for the single cell parametric tests using for LPR and potentiodynamic polarisation. The resistance of the bridge was measured to 679 Ohm, and the test was carried out with an initial 1 hour OCP followed by 1 hour of ZRA before adding 3.0 mg/l Pb(II) to one cell followed by ZRA for additional 18 hours.

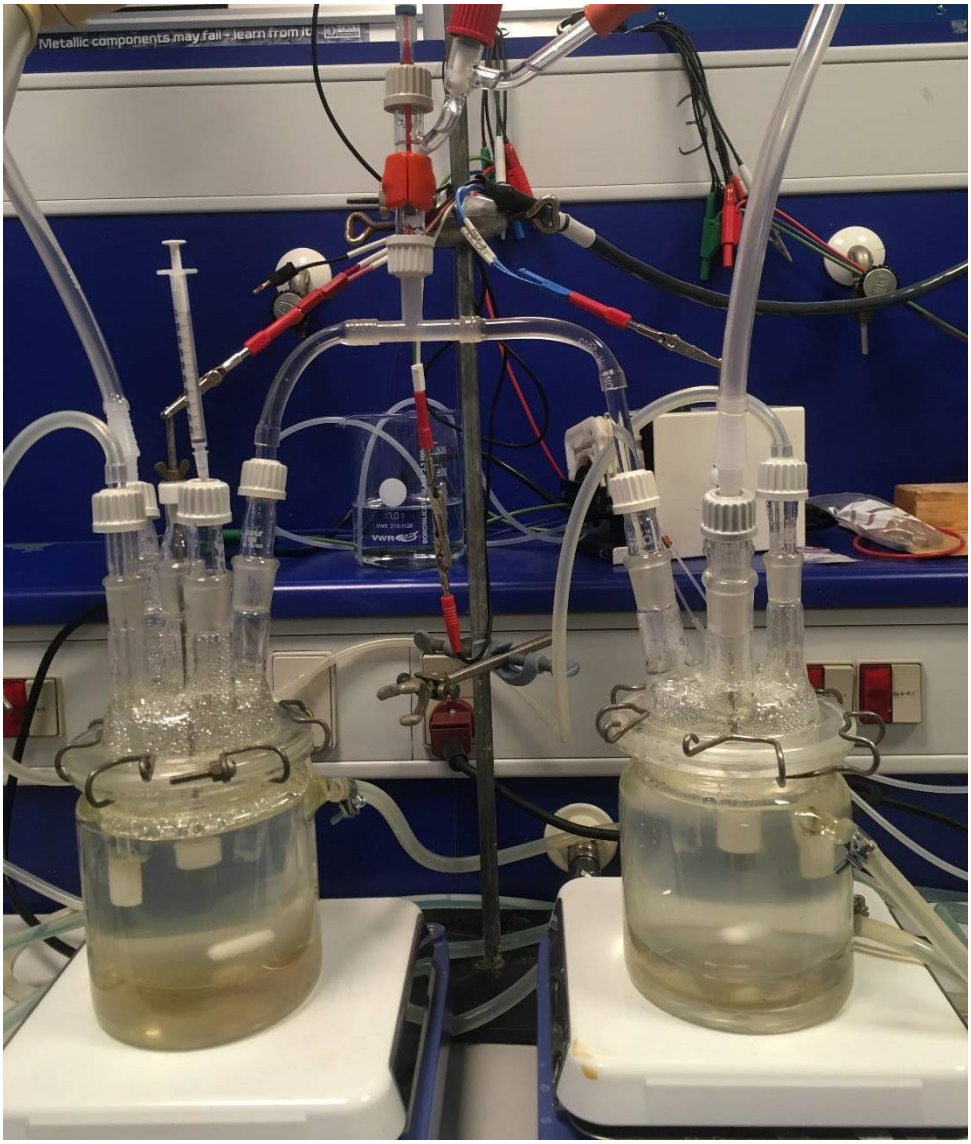

Figure 11. Galvanic corrosion current measurement (ZRA) for steel coupled to steel w. 3.0 mg/l Pb(II) using the initial double cell setup with salt bridge and central placement of the reference electrode.

An immediate response in the corrosion current was observed using the ZRA technique upon the addition of lead to one of the electrodes at 25 °C and 70 °C, when coupling steel and steel with lead added in solution. The measured current corresponding to corrosion rates of 0.012 and 0.029 mm/y for 25 and 70 °C, respectively. This indicates that the kinetics allow rapid reduction of Pb(II) to Pb, depositing the lead and corroding the steel as a result of the cathode and anode reaction:

$$Pb^{2+}\ 2e^{-} \rightarrow Pb \qquad \text{(cathode)}$$
$$Fe \rightarrow Fe^{2+} + 2e^{-} \qquad \text{(anode)}$$

However, slow normalisation of the current followed, indicating that the deposition process slows down as lead is being deposited. Thus, indicating the local galvanic cell on the steel surface where lead is directly deposited may be a slowly stabilising system. This is at least in the test conditions where lead ions is not continuously added to the solution. Here lead is consumed as it is reduces from Pb(II) to metallic lead as deposits, effectively reducing the concentration of Pb(II) and the measured current contribution from the cathode reaction above.

With testing at 25 and 70 °C, temperature showed to have great influence on the deposition kinetics and corrosion rate, as seen from Figure 12, with the effect increasing with temperature.

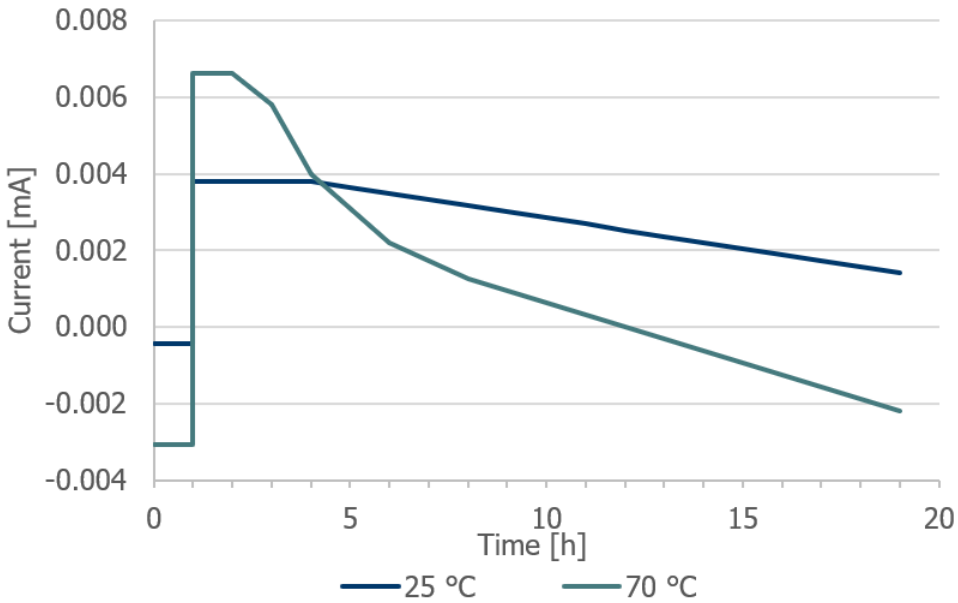

Figure 12. Galvanic corrosion current measurement (ZRA) for steel coupled to steel w. 3.0 mg/l Pb2+. Showing the current measured over time between the two cells at 25 and 70 °C. Deaerated with nitrogen. Simplified graph using averaged datapoints for better visibility.

While the trend shown in the simplified graph of Figure 12 was evident from the raw data, the recorded level of noise (after taking precautions to minimize this) has been attempted improved by removing the large resistance generating salt bridge and replacing the whole setup with a devanathan cell, as seen in Figure 13. Between the two half-cells was placed an anion exchange membrane (AEM) with the purpose of retaining the Pb(II) on one side while allowing anions such as chlorides to travel freely and having a low resistance connection between the two test samples for improved galvanic coupling.

Figure 13. Galvanic corrosion current measurement (ZRA) for steel coupled to steel w. 3.0 and 22.5 mg/l Pb(II) using a devanathan cell with AEM membrane as separator. Reference electrode positioned in one half-cell.

As this setup did not allow for mounting of a heat source, the tests were carried out at room temperature, in this case 23±2 °C and thus comparable to the previously tested 25 °C. As elevated temperatures could not be tested, the test was done with addition of 3.0 mg/l and 22.5 mg/l Pb(II). Resistance between electrodes was measured to only 24.5 Ohm (compared to 679 Ohm with the salt bridge). However, as can be seen from Figure 14, while recording a factor 10 larger current and showing less noise, this does not show the same clear response to the addition of lead at one hour of testing. Although some change in the current is observed a later shift in the opposite direction is seen for both Pb(II) concentrations before continuing in the initial direction.

The shift in current immediately after the addition corresponds to a corrosion rate of 0.017 and 0.024 mm/y for 3 and 22.5 mg/l Pb(II), respectively. Looking at the case with 3.0 mg/l Pb(II), this is very similar to the 0.012 mm/y obtained using the previous setup. However, where the previous setup would show a clear effect and subsequently go back towards zero this setup shows a larger response later on. If the current shift sustained here is evident of the corrosion current, a corrosion rate of 0.094 and 0.199 mm/y applies to 3.0 and 22.5 mg/l Pb(II) respectively. These rates do not correspond with the more theoretically determined rates for galvanic corrosion using potentiodynamic polarisation, and coupled with the changed response pattern, it may indicate incorrect data. The use of the AEM or the positioning of the reference electrode in one cell are suspected as possible causes for the poor measurement. We have learned that the double cell ideally should have been designed with a glass frit separator, having the reference electrode at the centre.

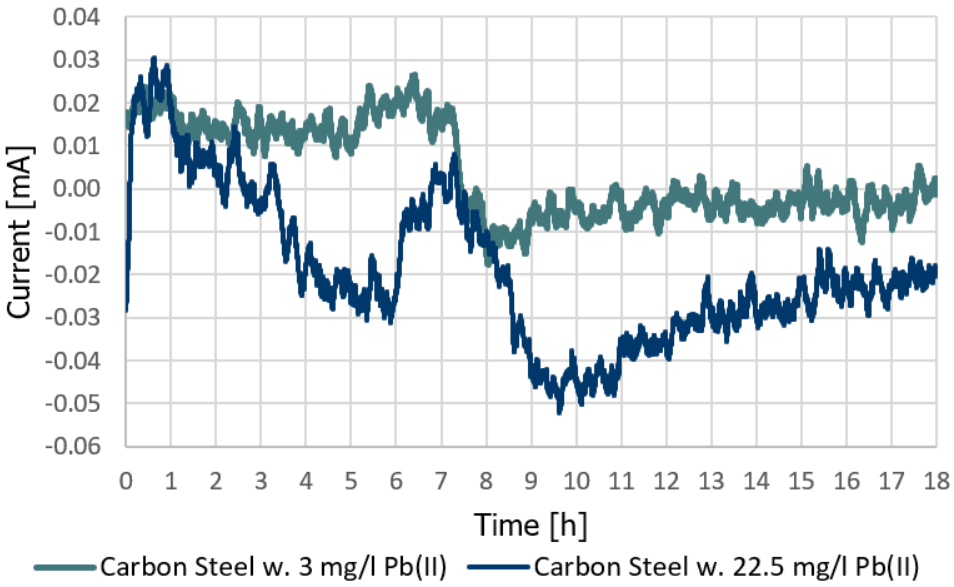

Figure 14. Galvanic corrosion current measurement (ZRA) for steel coupled to steel w. 3.0 and 22.5 mg/l Pb(II). Showing the current measured over time between the two cells at 23 °C deaerated with nitrogen. Depicting moving average of datapoints for better visibility.

1.4.4 Corrosion inhibitor

While the results of ZRA and the theoretical values for galvanic coupling showed discrepancies, the results from potentiodynamic polarisation and LPR showed good agreement, where LPR has the advantage that it is considered non-destructive, thus allowing for measuring corrosion rates over a longer period. This also allowing investigation of the effect of the rapidness with which lead may be depositing and shed additional light on the results of the polarisations and ZRA. In addition, the effect of the Nalco corrosion inhibitor (Nalco GEO942) used at Margretheholm has been investigated.

Information from HOFOR specified that the intended dosage level was 1 or 10 ppm. This shows more than a factor five reduction in corrosion rate with both 1 ppm and 10 ppm at 25 °C, calculated from polarisation curves illustrated in Figure 15 and 16, summarised in Table 3.5. At 70 °C, 1 ppm Nalco in solution yielded a factor two reduction in corrosion rate; however, 10 ppm unexpectedly showed an increase in corrosion rate, possibly due to the associated 100 mV increase in corrosion potential.

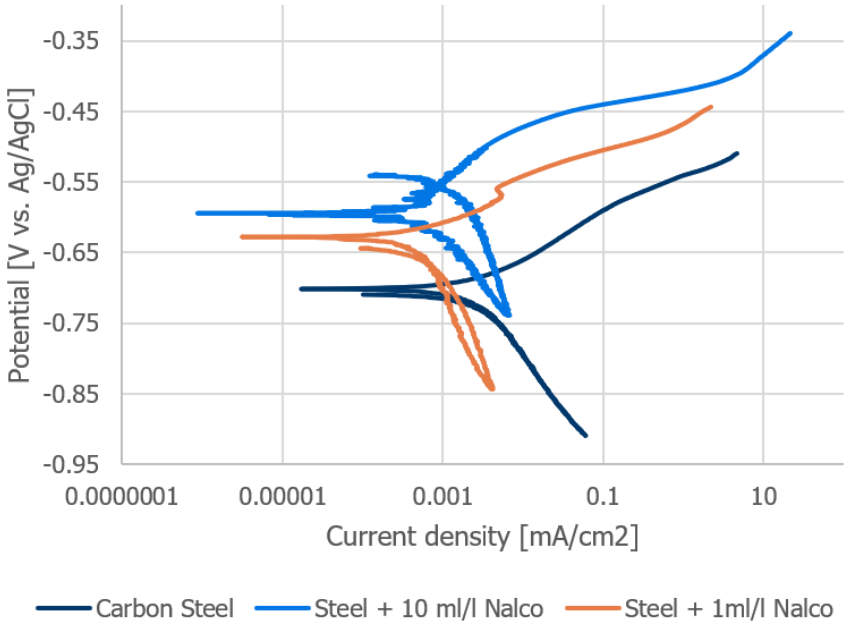

Figure 15. Cyclic polarisation of carbon steel with and without inhibitor (Nalco) in artificial brine at 25 °C. Deaerated with nitrogen.

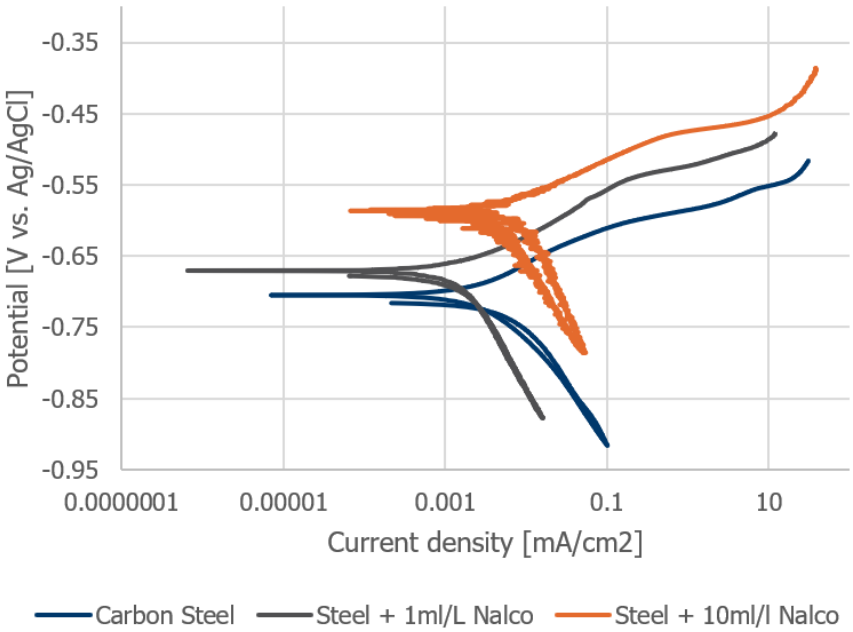

Figure 16. Cyclic polarisation of carbon steel with and without inhibitor (Nalco) in artificial brine at 70 °C. Deaerated with nitrogen.

Table 3.5. Corrosion rates calculated from cyclic polarisation, i.e. Tafel extrapolation on individual material polarisations curves.				
Material	Temp.	Electrolyte	E_{corr} [mV]	Corrosion rate [mm/y]
Carbon Steel	25 °C	Brine	-702	0.023
Carbon Steel	70 °C	Brine	-702	0.023
Carbon Steel	25 °C	Brine + 3.0 mg/l Pb(II)	-696	0.024
Carbon Steel	70 °C	Brine + 3.0 mg/l Pb(II)	-638	0.008
Carbon Steel	25 °C	Brine + 1 ml/l NALCO	-626	0.004
Carbon Steel	25 °C	Brine + 10 ml/l NALCO	-598	0.004
Carbon Steel	70 °C	Brine + 1 ml/l NALCO	-663	0.004
Carbon Steel	70 °C	Brine + 10 ml/l NALCO	-588	0.01

Reduction in corrosion rate at 25 °C, similar to that obtained from the polarisation technique, was recorded using LPR with and without lead in solution (Figure 17), giving a reduction of a factor two and three. The effect of the inhibitor showed to increase with time (Figure 18), likely due to acting after a film forming principle and kinetics of its deposition, further reducing the corrosion rate by almost an additional factor 3 (more than a factor 5 in total). These data were obtained with stirring (flow) but for the steel with lead in solution the flow showed to have an effect with a factor 2 increase in corrosion rate for steel with 3.0 mg/l Pb(II), while only a minor increase for steel with 22.5 mg/l Pb(II) in the brine. The results are summarised below in Table 3.6.

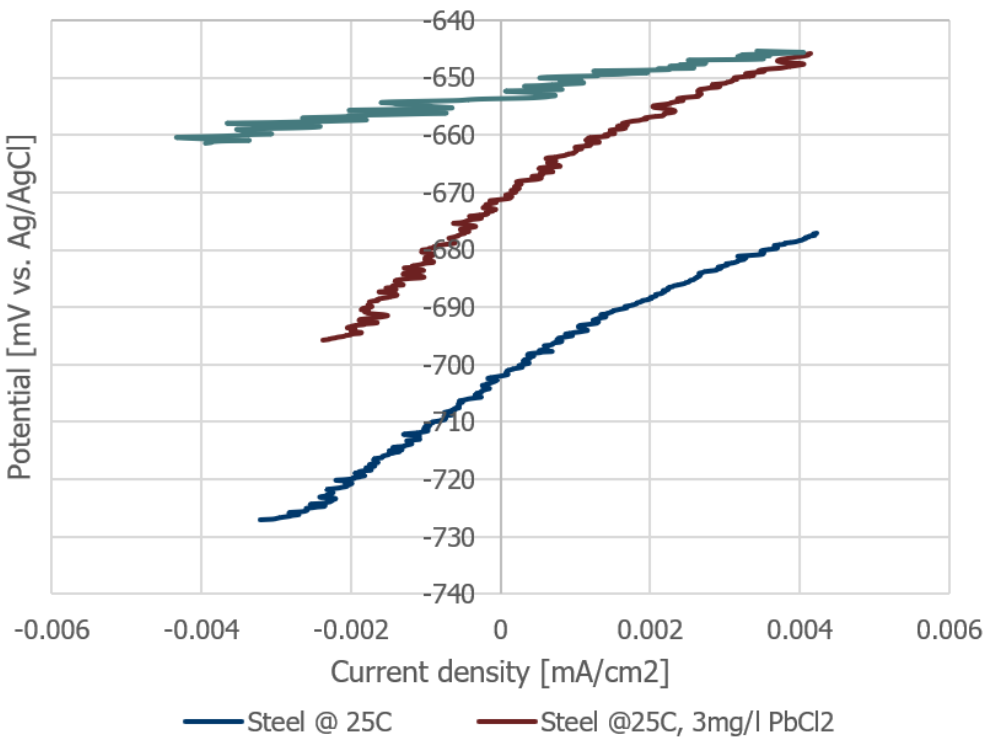

Figure 17. Linear polarisation resistance measured for carbon steel in artificial brine at 25 °C with 3.0 and 22.5 mg/l Pb(II) in solution. Deaerated using nitrogen.

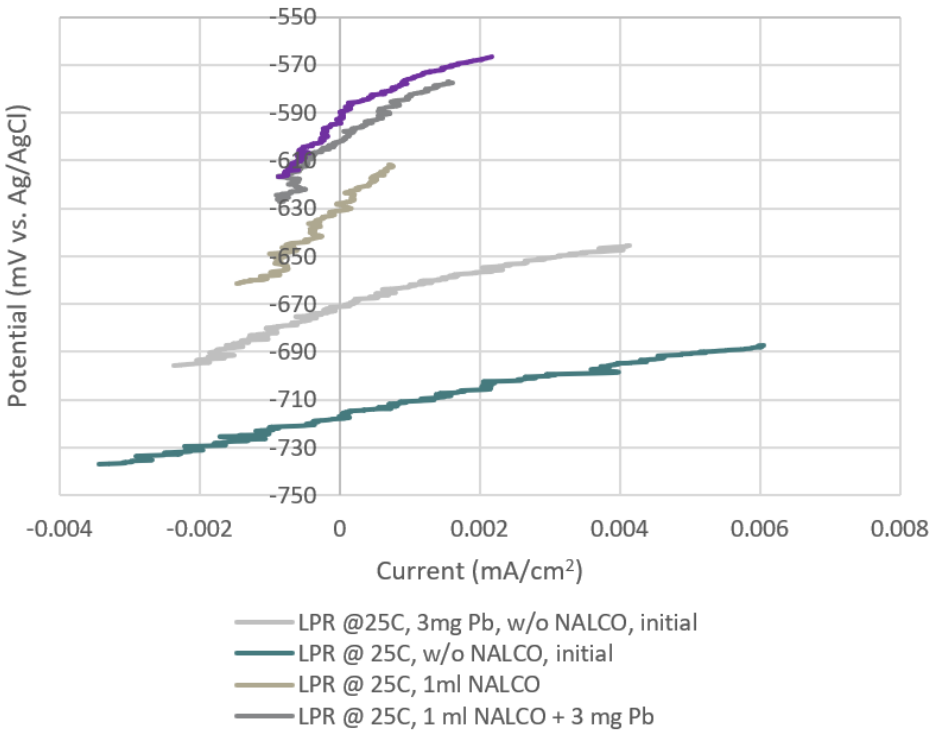

Figure 18. Linear polarisation resistance measured for carbon steel in artificial brine at 25 °C with 3.0 and inhibitor (Nalco). Deaerated using nitrogen.

Table 3.6. Corrosion rates measured using linear polarisation resistance.

Material	Temp.	Electrolyte	Corrosion rate [mm/y]
Steel	25 °C	Brine + 3.0 mg/l Pb^{2+}	0.027
Steel	25 °C	Brine + 22.5 mg/l Pb^{2+}	0.121
Steel	25 °C	Brine + 1 ml/l NALCO	0.01
Steel	25 °C	Brine + 1 ml/l NALCO + 3.0 mg/l Pb^{2+}	0.014
Steel	25 °C	Brine + 1 ml/l NALCO + 3.0 mg/l Pb^{2+}, after 3 h stirring	0.005
Steel	25 °C	Brine + 3.0 mg/l Pb^{2+}, stir OFF	0.051
Steel	25 °C	Brine + 22.5 mg/l Pb^{2+}, stir OFF	0.162

The effect of lead was further investigated under conditions mimicking the service conditions in the Margretheholm plant, with 70 °C and 70 bar, using an autoclave fitted with electrochemical electrodes. These tests were carried out in stages with the earlier tests trying out the principles are dialling in test period and parameters. Below in Figure 19 is shown the results from the final testing. Lead concentration goes from 3.0 mg/l to 22.5 mg/l after which 10 ml/l inhibitor is added. The effect of flow under these conditions are difficult to deduct but it is seen how the OCP increases with addition of lead along with the corrosion rate, while addition of inhibitor does not show any large influence the either.

The OCP and corrosion rate can be seen being at relatively low levels already prior to the addition of inhibitor and it is possible that without continuous addition of lead ions the corrosion rate is reduced and that addition of inhibitor at an earlier point would have yielded more evident results of its efficacy. The gap in the data makes it difficult to say with any certainty and is an unfortunate result of force majeure leading to the equipment being put out of service. While the data obtained following the gap is valid, further acquisition was not possible due to unreliable data transfer as a result of the initial incident. However, it is clear from the phase of deaeration that both OCP and corrosion rate is reduced with decreasing oxygen content, just as expected, and that the presence of Pb(II) ions in the brine will lead to increased corrosion rate regardless of the pressure and temperature range of 1-70 bar and 25-70 °C.

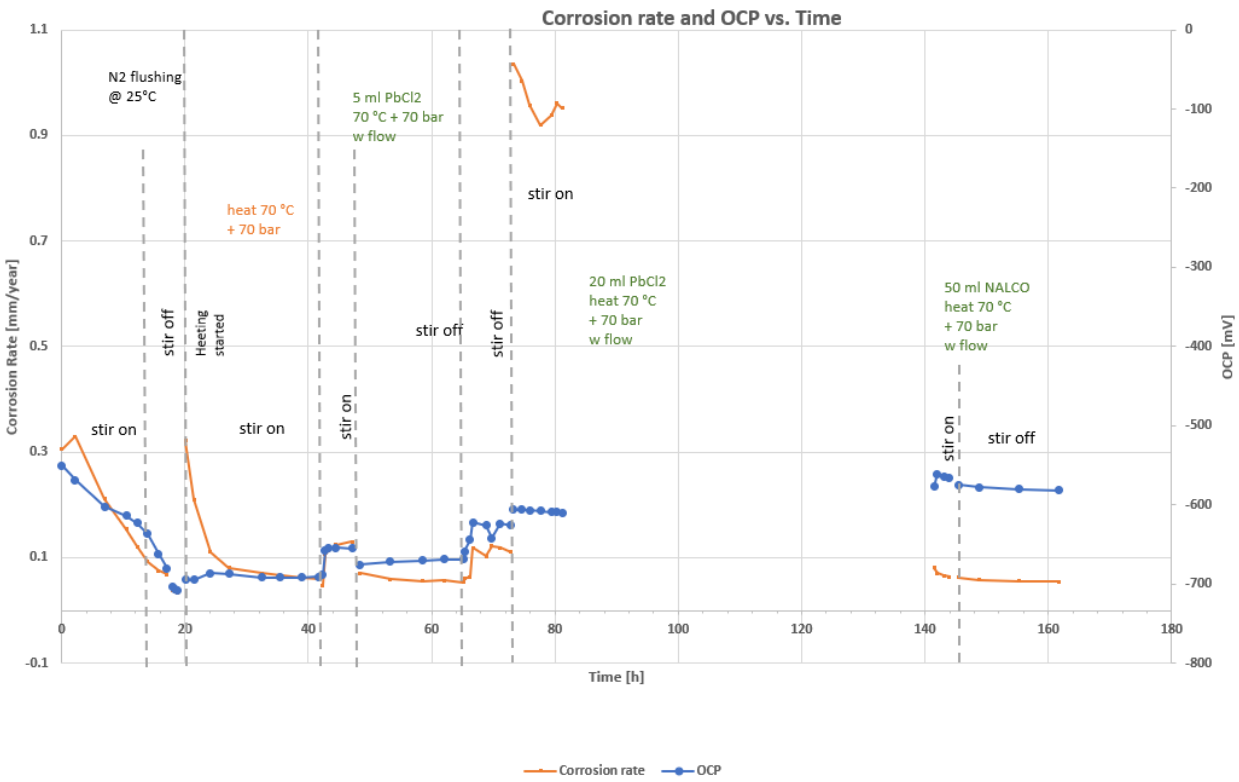

Figure 19. Corrosion rate obtained using linear polarisation resistance and open circuit potential (OCP) in artificial brine at varying temperature and pressure.

1.4.5 Calculations on galvanic element from lead deposition

The Principal Component Analysis (PCA) in WP1 indicates, that galvanic corrosion due to lead is mainly a problem in highly saline brine solutions (>100.000 mg/Cl). The encircled plants in Figure 20 experience both high corrosion rate and a high chloride content together with lead in the brine.

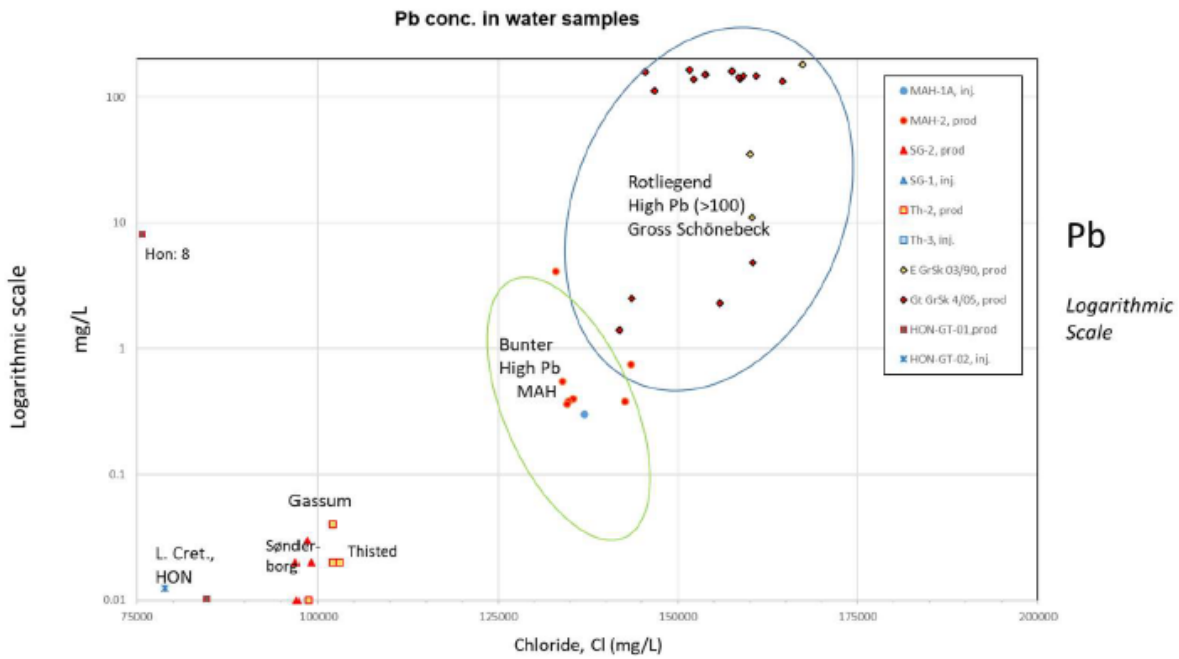

Figure 20. Pb concentration as a function of Cl concentration for key sites.

To quantify the distance of the galvanic element, occurring due to lead deposition, mathematically modelling has been applied using formulas for cathodic protection [11].

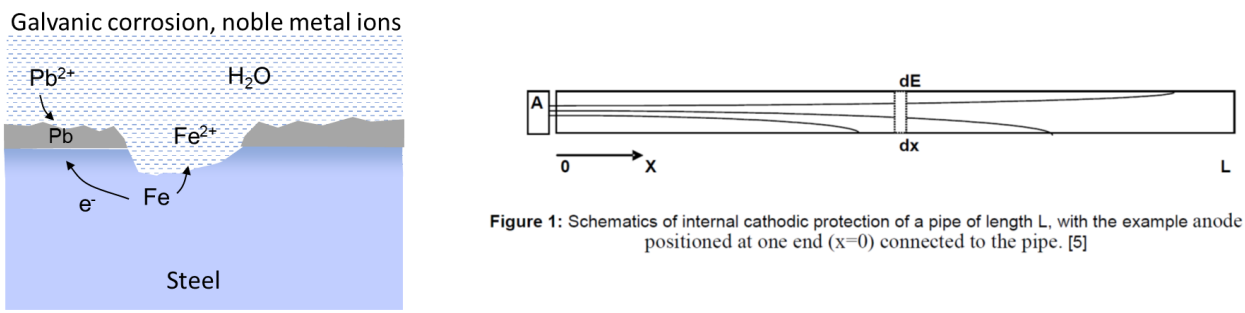

Figure 21. Mechanism of galvanic corrosion of steel due to Pb (left). Basis for the mathematical model showing a pipe with a defect A (anode) and the resulting distribution in potential (dE) as function of the distance (dX) (right).

The following assumptions are made for the calculations:

Pipe diameter, D:	0.2 m	Typical size in geothermal plant
Anode resistance, R_a:	0 ohm	A circular defect is assumed
Driving voltage, ΔE:	150 mV	Obtained from electrochemical tests
Resistivity, ρ:	0.03 ohm m	Margretheholm
	0.04 ohm m	Sønderborg and Thisted
	0.3 ohm m	Seawater
Current density, i	1 $\mu A/cm^2$ = 10 mA/m^2 from ZRA tests	

Equation (1) used for calculation active pipe length:

$$L = D\left(\frac{(-\pi D R_a i) + \sqrt{(\pi D R_a i)^2 + \frac{8\rho i(\Delta E)}{D}}}{4\rho i}\right) \quad (1)$$

Table 3.7. Result of calculations.

Water type	Resistivity [ohm m]	Active pipe length in galvanic element [a] L [m]	L/D [b]	Total cathode area, 2xL [c] [m²]	Corrosion rate of bare area (cm²) [d] 628 [mm/y]	3142 [mm/y]
Margretheholm	0.03	7.1	35	8.9	3.3	0.7
Sønderborg & Thisted	0.04	6.1	31	7.7	2.8	0.6
Seawater	0.3	2.2	11	2.8	1.0	0.2

a. Calculated from equation (1).
b. Length/diameter ratio.
c. Assumes that Pb cathode appears both directions form anode (coating defect).
d. Corrosion rate calculated for two defect sizes, a circular band 10 cm wide and 50 cm wide, respectively.

The resistivity of the brine obviously has a great impact on the extent of the galvanic element. Going from seawater to brine with high salinity extends the galvanic element by a factor 3. It means that the galvanic elements extents 35 pipe diameters away in both directions from the defect. Accordingly, the corrosion rate of the bare area increases by a factor 3. However, the difference in resistivity between Margretheholm and Sønderborg/Thisted is negligible. Therefore, the difference in corrosion behaviour observed in the PCA cannot entirely be explained by the drop in resistivity from increase chloride, giving a greater coverage of galvanic element. Other mechanisms are suspected to interact, i.e. complexing of chloride with either lead or iron, leading to altered solubility of scaling behaviour of the metals.

1.5 Corrosion resistant alloys

Corrosion resistant alloys (CRA), here specifically L80-13Cr (commonly used for tubings in the oil and gas industry) and AISI 316L, where investigated in regard to their corrosion performance in the artificial Margretheholm brine with and without lead much like seen for the carbon steel in the previous sections. For the corrosion resistant alloys, specifically AISI 316L, was also investigated the influence of oxygen ingress and whether this would affect the performance by raising the aggressivity by raising the potential.

1.5.1 Effect of lead in solution

Measuring OCP for L80-13Cr and AISI 316L with and without lead in solution reveals little to no effect on the potential of the two CRAs with the presence of lead at 25 °C (Figure 22). This is to no great surprise, when looking at the potential of lead itself in comparison to the two. Here lead has a significantly lower potential than both CRAs, and thus no driving force for metallic lea d to deposit on these. The lack of driving force is supported by the absence of lead on the AISI 316L surface when examined in scanning electron microscope post testing. A similar picture is seen at 70 °C (Figure 23). At this elevated temperature, the potential of L80-13Cr and lead both drop roughly 50 mV. AISI 316L drops around 25 mV but more importantly shows instability in the environment. This is noted by the occasional drops on the curve, indicating breakdown of the passive film followed by

repassivation. With the addition of lead in solution, AISI 316L appears to be depolarised, while L80-13Cr show no difference from when lead is absent. Thus, passive stainless steel (AISI 316L) will behave as cathode and lead as anode in the artificial brine.

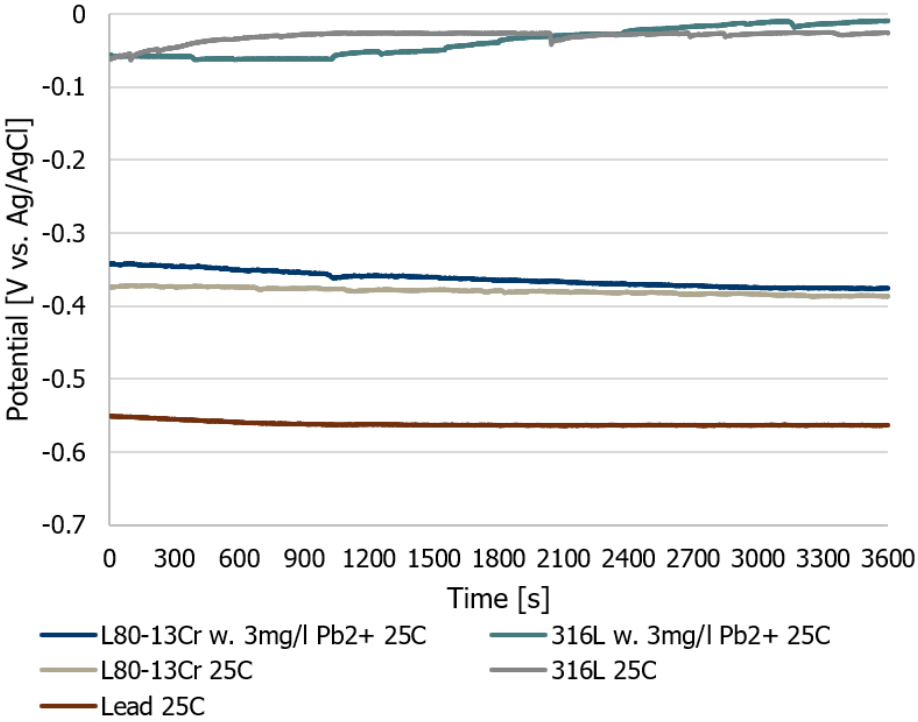

Figure 22. Open circuit potential recorded for L80-13Cr and 316L with and without Pb(II) in artificial brine at 25 °C. Deaerated using nitrogen.

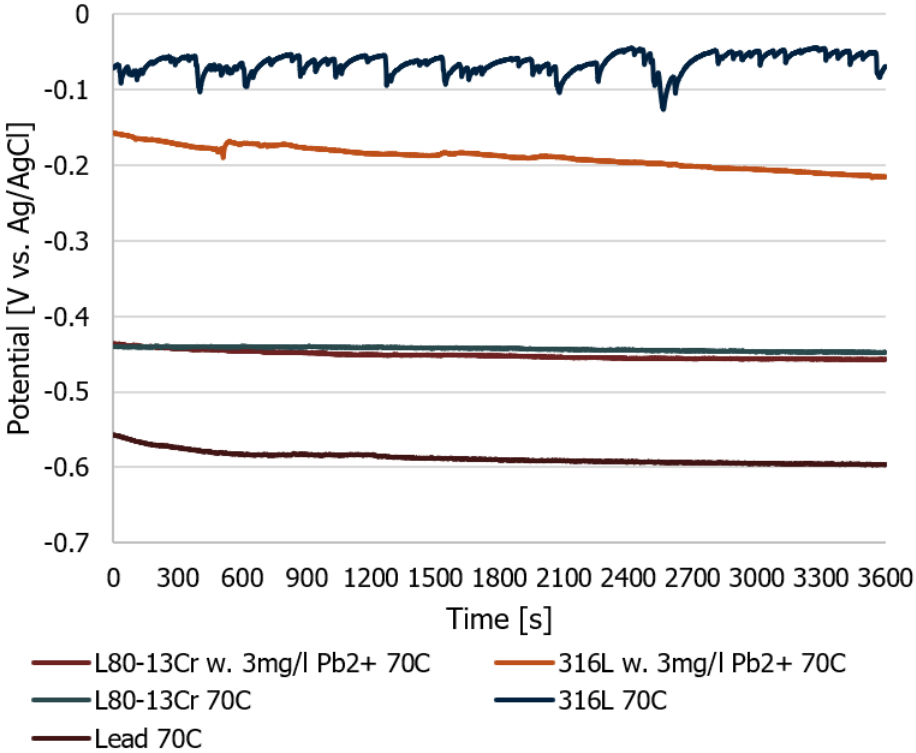

Figure 23. Open circuit potential recorded for L80-13Cr and 316L with and without Pb(II) in artificial brine at 70 °C. Deaerated using nitrogen.

While lead in solution showed no effect on the open circuit potential of AISI 316L at 25 °C, it is evident, using potentiodynamic polarisation, that lead reduces the pitting potential (E_{pit}) yielding it more susceptible to initiation of localised corrosion (Figure 24). However, at 70 °C there are indications that AISI 316L may benefit from the presence of lead. The pitting potential of AISI 316L increases and passive current is lower with the presence of lead in solution (Figure 25). This effect may be a result of the higher temperature leading to a more rapid deposition of a thin layer of lead on the surface. It is possible that lead either adsorbs to the passive film on the stainless steel or it forms a substance with poor solubility, e.g. lead oxide or lead sulphide on the surface impairing the steel reacting with the solution. In regards to the repassivation potential (E_{rp}), lead does not appear to have a significant effect at neither 25 °C nor 70 °C. L80-13Cr shows no passivation of the steel at either test temperatures, and starts pitting immediately as it is polarised anodically. Like it was the case with OCP, lead in solution appears to have no effect on the corrosion behaviour.

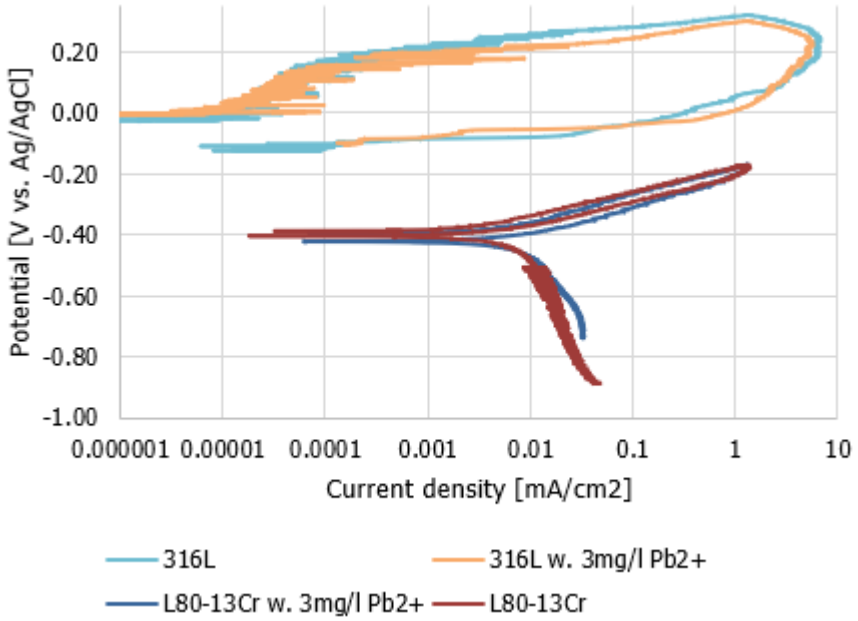

Figure 24. Cyclic polarisation curve for L80-13Cr and 316L with and without Pb(II) in artificial brine at 25 °C. Deaerated using nitrogen.

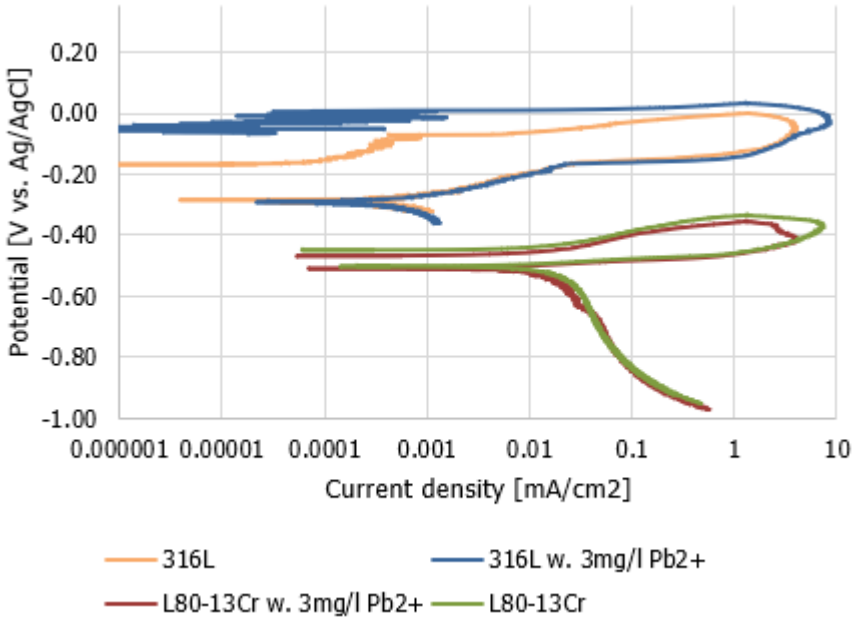

Figure 25. Cyclic polarisation curve for L80-13Cr and 316L with and without Pb(II) in artificial brine at 70 °C. Deaerated using nitrogen.

Based on the results obtained via the OCP and potentiodynamic polarisation, and the key data summarised in Table 3.8 below, it is evident that AISI 316L exhibits a behaviour indicative of borderline compatibility in the brine, although the presence of lead appears to inhibit corrosion at 70 °C, it is clear AISI 316L is not suitable in the warm geothermal brine, as variation in lead content will occur and this positive effect cannot be guaranteed. In the case of L80-13Cr, the low open circuit potential and the immediate corrosion occurring when polarised anodically makes it clear that it will not be suitable for use in either cold or warm brine and will be no improvement over the low alloyed carbon steel. As discussed in the next section, the tolerance to oxygen ingress is too low.

Table 3.8. OCP, pitting (E_{pit})and repassivation (E_{rp}) potentials with and without Pb(II) for CRAs. Potentials measured vs. Ag/AgCl.

Material	Temp.	Electrolyte	OCP [V]	E_{pit} [V]	E_{rp} [V]
Stainless Steel 316 L	25 °C	Brine	-0.027	0.256	-0.081
Stainless Steel 316 L	70 °C	Brine	-0.056	-0.062	-0.261
Stainless Steel 316 L	25 °C	Brine + 3.0 mg/l Pb^{2+}	-0.011	0.213	-0.059
Stainless Steel 316 L	70 °C	Brine + 3.0 mg/l Pb^{2+}	-0.213	0.008	-0.268
L80-13Cr	25 °C	Brine	-0.386	-0.339	-0.397
L80-13Cr	70 °C	Brine	-0.447	-0.431	-0.500
L80-13Cr	25 °C	Brine + 3.0 mg/l Pb^{2+}	-0.376	-0.359	-0.419
L80-13Cr	70 °C	Brine + 3.0 mg/l Pb^{2+}	-0.457	-0.458	-0.506

1.5.2 Effect of oxygen ingress

With oxygen ingress being a natural concern for geothermal systems using carbon steel tubing, it is relevant to study the effect of such oxygen contamination for CRA too, namely AISI 316L. While only minute concentrations of oxygen is needed to form the protective chromium oxide layer on the steel, oxygen is a well-known element for raising the potential. What interesting is, if expected oxygen ingress may be sufficient to raise the potential of the stainless steel surface causing it to corrode.

There is plenty of experience from oil and gas production about CRAs for produced water and aquifer water injection. Such systems are comparable with geothermal doublets. An exact limit for dissolved oxygen is not available, but <10 ppb is often mentioned for 13Cr stainless steel and <20 ppb for more resistant alloys [12].

A customised setup was built. The oxygen content was controlled by contaminating pure nitrogen purging gas with small amount of air (Figure 26).

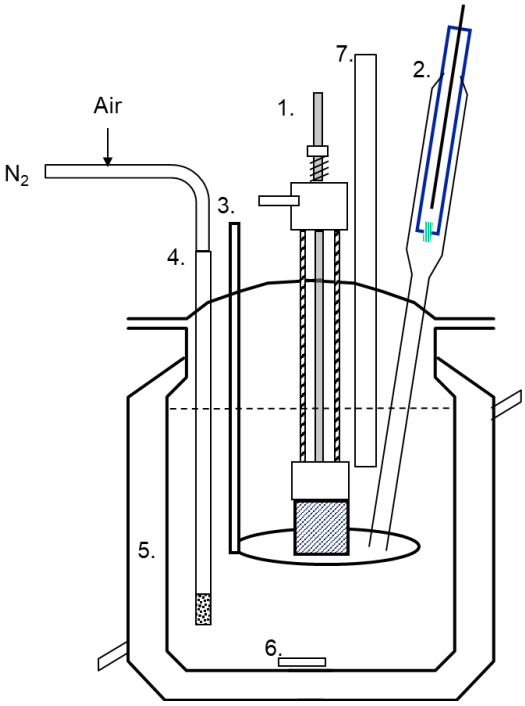

Figure 26. Setup for DO measurement. 1. Water-flushed pitting electrode 2. Ag/AgCl reference electrode. 3. Platinum electrode 4. Gas purge 5. Heating jacket 6. Stirrer 7. DO sensor WTW 3510

This is investigated by stepwise increase of dissolved oxygen (DO) in the brine while measuring the OCP of AISI 316L and a platinum electrode. This was carried out at 25 and 50 °C due to temperature limitation of the oxygen probe, and an example of the curve obtained by such test can be seen in Figure 27.

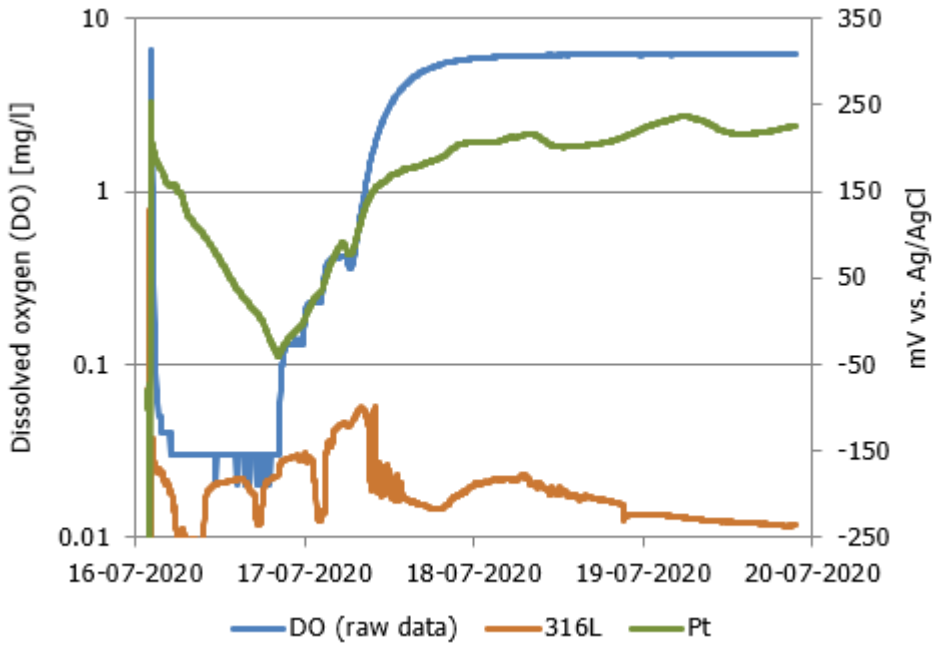

Figure 27. Open circuit potential of AISI 316L and platinum (Pt) with increasing dissolved oxygen (DO) in artificial brine at 50 °C.

As can also be seen from the above curves in Figure 27, AISI 316L experienced activation issues (a result of the borderline compatibility) while the platinum electrode showed potential increase consistent with the stepwise increase in DO. Common for both is however that some increase is observed in the open circuit potentials, and summary of these data are depicted in Figure 28. In the case of AISI 316L a clear trend cannot be seen, as reduced potentials are sometimes seen for increased DO. While platinum also show unexplainable drop in potential between DO content of approximately 0.01- 0.1 mg/l the overall trend is clear, meaning increased oxygen DO will increase the potential at the surface of the stainless steel, with platinum showcasing the worst possible potential increase.

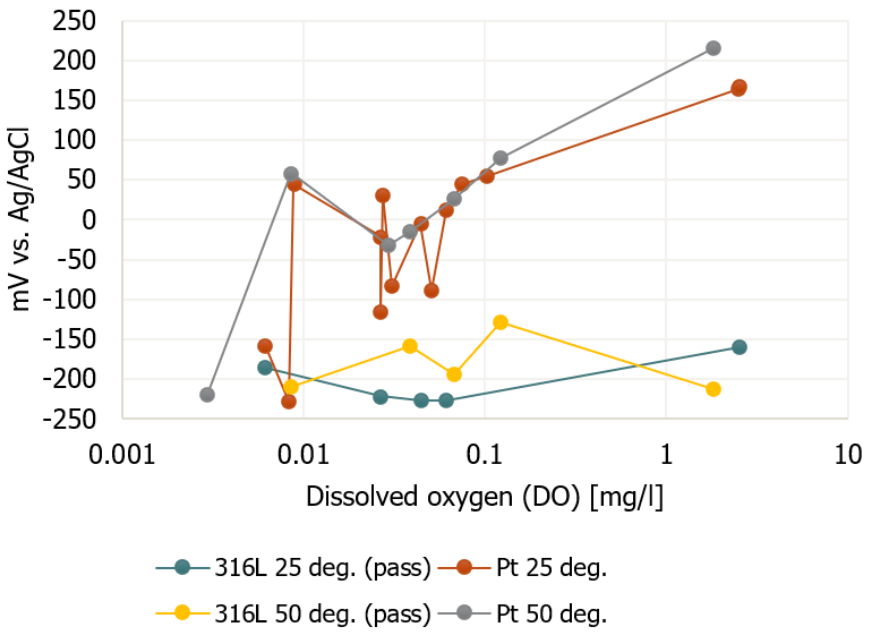

Figure 28. Open circuit potential for AISI 316L as function of dissolved oxygen in artificial brine at 25 and 50 °C

With DO ranging from 0.006 - 2.5 (saturated) mg/l (6 - 2500 ppb), the potential increase on the stainless steel is not sufficient to cause immediate pitting, when comparing the recorded potentials (-228 – -129 mV) with the previously determined pitting potentials (-62 – 256 mV).
To further determine the susceptibility to pitting as function of DO content, the pitting potential of AISI 316L was determined with fully oxygen saturated artificial geothermal brine and compared to that of the deaerated at 25 °C (Figure 29).

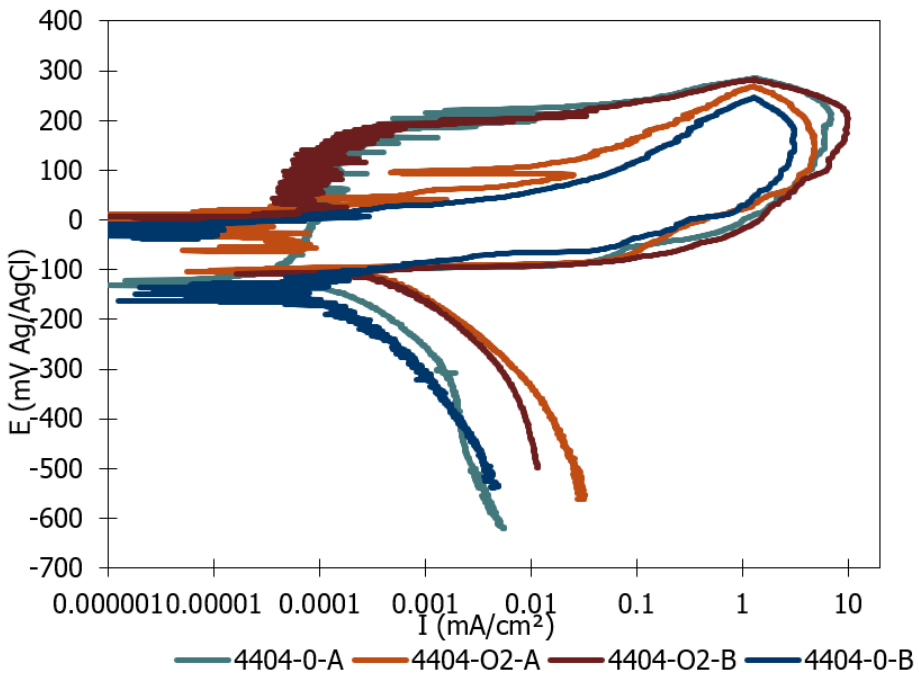

Figure 29. Cyclic polarisation curve for AISI 316L with artificial brine at 25 °C deaerated with nitrogen and saturated with dissolved oxygen.

Although there are clearly variations in the behaviour of AISI 316L, the curves with and without oxygen saturation looks the same (4404-0-A equal to 4404-O2-B and 4404-O2-A equal to 4404-0-B, with “0” marking the deaerated and “O2” the oxygen saturated. Thus, it appears there is no difference in pitting potential for AISI 316L with different degree of oxygen ingress, which is underlined by the similarities in pitting and repassivation potentials summarised in Table 3.9. This may also be a result of the already borderline behaviour of AISI 316L in the brine.

Table 3.9. Epit and Erp with varying DO concentration. Potentials measured vs. Ag/AgCl.

Reading	4404-0-A	4404-O2-A	4404-O2-B	4404-0-B
E_{pit}, mV Ag/AgCl	199	76	205	57
E_{rp}, mV Ag/AgCl	-98	-92	-97	-85

1.6 Galvanic effect of CO_2

The effect of CO_2 gas in saline waters in respect to corrosion of low alloyed steel and stainless steels are well documented from the oil and gas industry [13]. Because of this, the work carried out under PERFORM focused on a different angle. With temperature and pressure changing throughout the system the dissolvability and corrosivity of the CO_2 may change with it, and with the brine being an extremely well conducting electrolyte (section 3.2.5) the possibility of CO_2 leading to galvanic elements in the pipe system.

Testing was carried out using the zero resistance amperometry (ZRA) in the same devanathan cell utilized in the investigation of galvanic coupling due to lead deposition. In the case of CO_2, separation of the two half-cells were done using filtering paper. This provided sufficient separation between the cell purged with CO_2 from the one purged with N_2. Control using pH measurements revealed the efficiency of the separator with pH 3.77 and pH 5.86, respectively, after end testing. In comparison the virgin synthetic brine has a pH of 5.82 at the same ambient temperature of 23±2 °C. Resistance between electrodes was measured to 24.5 Ohm.

Figure 30 shows the coupling between carbon steel in brine deaerated with N_2 and carbon steel in brine saturated with CO_2. Initial recording of open circuit potential shows that carbon steel has a more noble potential when purged with N_2 than with CO_2. Thus, corrosion will more readily occur on the carbon steel in CO_2. This also coincides with the measured current showing current running with corrosion from the carbon steel in CO_2. The current gradually decrease over time, likely as carbonates build up on the surface but also as the carbon steel in brine purged with N_2 progresses to corrode as the depolarisation from the coupling is not sufficient to cathodically protect the carbon steel in this environment. Taking the average measured current over the test period, the corrosion rate of the carbon steel in CO_2 purged brine is estimated to 0.09 mm/y, when coupled to carbon steel in brine with more limited cathode reactions for the corrosion process.

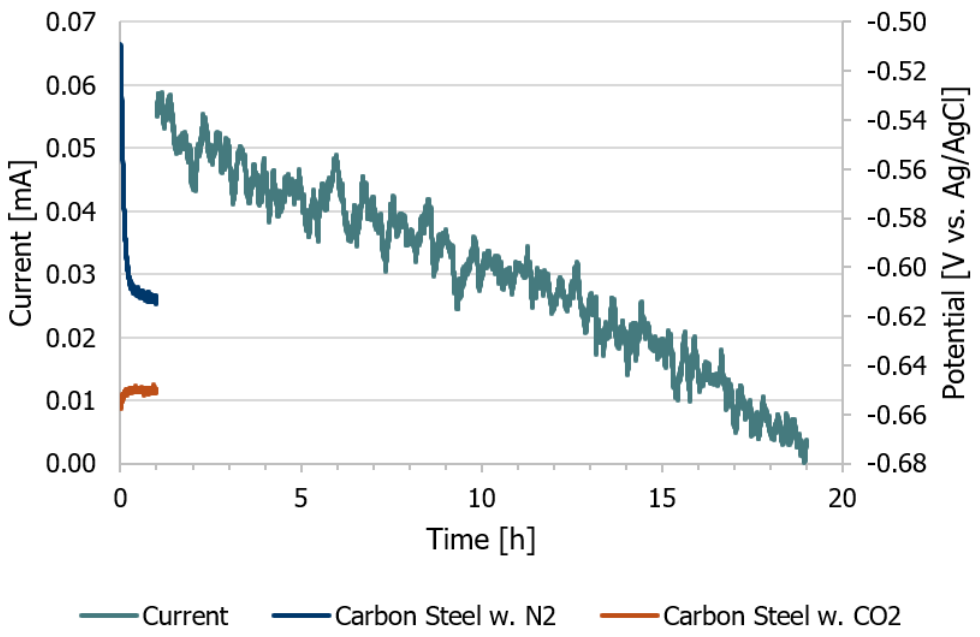

Figure 30. Galvanic corrosion current measurement (ZRA) for steel coupled to steel in brine purged with nitrogen and carbon dioxide. Showing OCP of each prior to measuring the current over time between the two cells. Depicting moving average of datapoints for better visibility.

Should CRA's, here AISI 316L, be chosen for components in the system the coupling between the stainless steel and carbon steel and the effect of CO2 has been investigated using the same approach. Figure 31 shows the coupling between carbon steel and AISI 316L where both half-cells are initially purged with nitrogen. Here, corresponding to the previous results, it is evident that AISI 316L has a significantly more noble potential in the brine than carbon steel. The effect of the galvanic bimetallic coupling shows in the measured current, yielding an estimated corrosion rate of the carbon steel of 0.173 mm/y in nitrogen purged conditions. With the introduction of CO_2 in the system, replacing nitrogen at about 3 hours into the test, a clear increase in measured current can be observed. This current corresponds to a corrosion rate of the carbon steel of 0.384 mm/y, when averaging the current for the remainder of the test. Thus, evident that the corrosion rate increases as CO_2 enters the system under deaerated (oxygen free) conditions.

The corrosion rate for carbon steel alone, calculated using NORSOK M-506, is 4.2 mm/y under the same conditions (pH 3.77, 1 bar CO_2). Thus, the corrosion contribution from the galvanic coupling to the more noble AISI 316L is only a moderate increase with 0.384 mm/y (9 % increase).

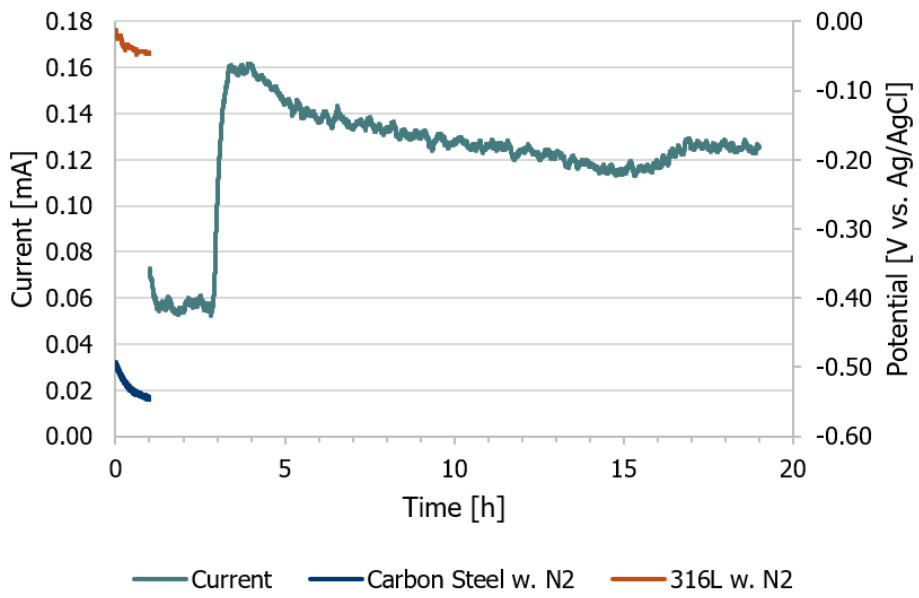

Figure 31. Galvanic corrosion current measurement (ZRA) for steel coupled to stainless steel in brine purged with nitrogen and subsequently carbon dioxide in both cells (after two hours of ZRA measurement). Showing OCP of each material prior to measuring the current over time between the two cells. Depicting moving average of datapoints for better visibility.

The increase in corrosion rate of the carbon steel when coupled with AISI 316L in CO_2 saturated brine may be a result of the carbon steel's reduction of corrosion resistance rather than the introduction of a possible cathodic reaction on the stainless-steel surface. Tests conducted with the coupling between carbon steel and AISI 316L where both half-cells are initially purged with nitrogen and the half-cell with AISI 316L subsequently with CO_2, show a similar rise in measured current upon introducing CO_2. With nitrogen in both half-cells the corrosion rate of the carbon steel is in this case estimated to 0.070 mm/y. In time, after introduction of CO_2 to the AISI 316L sample, the average current measured give an estimated 0.283 mm/y corrosion rate of the carbon steel it is coupled to. This shows that the introduction of CO_2 does indeed allow for AISI 316L to function as a cathode in coupling with carbon steel. The measured increase to peak value is almost the same under the conditions depicted in Figure 31 and Figure 32, indicating that the cathode reactions on AISI 316L is the driving force although the response is more immediate when CO_2 is present at both materials.

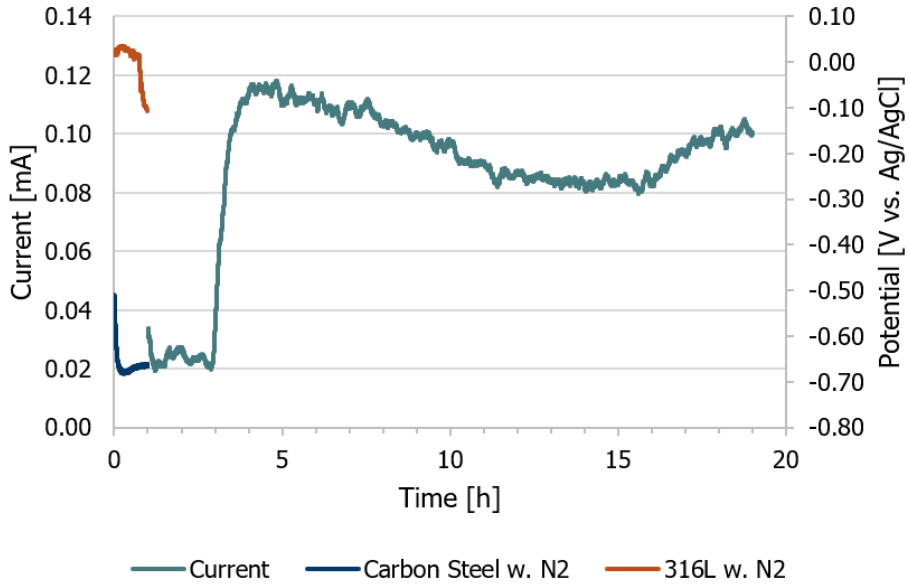

Figure 32. Galvanic corrosion current measurement (ZRA) for steel coupled to stainless steel in brine purged with nitrogen and subsequently carbon dioxide to the stainless steel cell (after two hours of ZRA measurement). Showing OCP of each material prior to measuring the current over time between the two cells. Depicting moving average of datapoints for better visibility.

4 Discussion and conclusions

The specific conditions for the Danish geothermal plants have been covered, having steel as the main construction material.

With carbon steel being a commonly used material in geothermal plants, the observation of deposition of more noble species present in the brine onto the surface of these steel parts, such as lead at Margretheholm and lead in combination with copper at Groß Schönebeck, is widely seen and documented in other studies as part of the PERFORM project [1-2]. At Margretheholm the deposition of lead is believed to cause galvanic corrosion of the carbon steel leading to penetrating corrosion. Here the deposition introduces a cathode reaction for dissolution of the steel in spite of otherwise oxygen free conditions. With literature on the electrochemical testing of lead and in combination with steel in salt brines, such as geothermal brine, is scarce a major part of the laboratory testing has focused on developing test methods, e.g. double-cells for measuring galvanic currents. The corrosion behaviour of carbon steel and metallic lead in artificial geothermal brine has been investigated in different parametric tests, varying temperature and the interaction with varying concentrations of lead in solution (0.0, 3.0 and 22.5 mg/l Pb(II)) added as lead chloride ($PbCl_2$).

These studies showed that lead is more noble than steel with and without lead in solution, thus explaining the galvanic dissolution of steel. It also showed that while the temperature (25 and 70 °C) has no significant effect on the corrosion rate of carbon steel in lead-free brine it had a large effect with 22.5 mg/l Pb(II) in solution. The low concentration with 3.0 mg/l showed no effect at 25 °C and a deviating reduction in corrosion rate at 70 °C. The reason for this reduction is not known and looking at the general coherence between increased temperature and increased effect of lead in solution for the carbon steel, all points to the influence of a higher lead deposition rate at high temperature. At the Margretheholm site, lead deposits are mainly observed in the hot lines from for the production well.

Estimated corrosion rates based on Evans diagrams, having carbon steel as anode plotted with various combinations of cathodes, showed increasing corrosion rate with increasing lead concentration and the highest corrosion rate with metallic lead as cathode in Pb(II) containing brine. Thus, indicating the ongoing process in the geothermal tube systems with lead depositions and lead in solution leading to high corrosion rates of the adjacent carbon steel.

Double-cell zero resistance amperometry investigating the galvanic effect of a coupling between carbon steel and carbon steel with deposition of lead from solution showed great influence of temperature, as measured current greatly increased from 25 to 70 °C. This shows that with increased temperature comes increased deposition and corrosion rate. While attempted refinement of the cell did not enable temperature control, this showed a similar effect of increased concentration of Pb(II), leading to the conclusion that the deposition of lead is what drives the corrosion of carbon steel when present as ions in solution. This corrosion rate can then see increase via either concentration of Pb(II) or temperature. The former supplies more ions to react leading to a more rapid formation of lead deposits and the latter affects the kinetics leading to the same.

With Margretheholm dispensing corrosion inhibitor (Nalco GEO942) prior to lockdown of the plant, the effect of such inhibitor was also investigated. Investigation in to this showed that the dosage of corrosion inhibitor has only limited effect (2-5 times reduction in corrosion rate) as seen in both formerly acquired on-site measurements [8] and laboratory testing. Linear polarisation resistance measurements showed that the efficacy of the inhibitor increased with time, likely due to having given the inhibitor time to adsorb to the surface or consumption of the lead in solution. Stirring showed to have a positive effect when lower concentration of Pb(II), with a doubling in corrosion rate occurring when stagnant. This may be due to supply of inhibitor to the sample surface slowing down as the flow stops. Interestingly efficacy declined in a system without Pb(II) with increase in inhibitor from 1 to 10 ml/l at 70 °C. This is possibly explained by the increase in potential by adding the inhibitor. While the use of inhibitor has been briefly touched in this study, a further in-depth investigation into mechanics and alternative inhibitors should be carried out for the various complex geothermal brines.

An alternative to adding inhibitor to mitigate the corrosion is the selection of another more suitable material, typically corrosion resistant alloys (CRA) such as AISI 316L are used in conditions where carbon steel is not sufficient, but also the corrosion resistant alloy L80-13Cr that is widely used in the oil and gas industry is investigated. Open circuit potentials showed that lead was electrochemically less noble than both CRAs and thus no galvanic driving force for the deposition of lead onto the surface of these steels. Investigation, using scanning electron microscopy on an AISI 316L sample post exposure, showed no lead on the surface. This corresponds with the findings of Stoljarova et al. where lead could not be found on the surface even after 30 days of exposure [2]. It is evident that AISI 316L exhibits a behaviour indicative of borderline compatibility in the brine, although the presence of lead appears to inhibit corrosion at 70 °C, as variation in lead content will occur this positive effect cannot be guaranteed. In the case of L80-13Cr, the low open circuit potential and the immediate corrosion occurring when polarised anodically makes it clear that it will not be suitable for use in either cold or warm brine and will be no improvement over the low alloyed carbon steel. The results for AISI 316L is in contrast to the ones by Stoljarova et al. that found EN 1.4404 (AISI 316L) to perform well in both lead free and Pb(II) containing brine [2]. Differences between the two studies is the brine itself (Margretheholm and Groß Schönebeck) and temperature (25-70 °C and 150 °C). With AISI 316L exhibiting the borderline behaviour it is not unlikely that changes in brine chemistry and in combination with temperature can yield a different result. In the Margretheholm brine the safety margin is not very big, considering the strict limits to oxygen ingress.

While oxygen ingress appears to cause corrosion on the carbon steel at Sønderborg and on-site data from Thisted does show some increase during shutdown procedure as well, investigation into the effect of oxygen ingress on the corrosion performance of AISI 316L did not show a significant difference in open circuit potential or pitting potential with increasing amount of dissolved oxygen. Additionally, it did not appear the raise in potential by oxygen was sufficient to cause pitting, although the potential raise on a platinum electrode under same conditions show a worst-case scenario capable of raising the potential sufficiently to initiate pitting. However, like described by Stoljarova et al., the low repassivation potential shows that once corrosion has initiated it may not stop again.

No damage has been reported for the AISI 316L stainless steel parts in the plants today. This is because all parts are in contact with carbon steel or iron anodes. However, upgrading entire pipe systems and well tubing to stainless steel is not yet viable.

While studying the effect of CO_2 on the coupling of carbon steel and CRAs (AISI 316L) does not give further direct insight to the corrosion performance of AISI 316L in the geothermal brine, it reveals that the presence of CO_2 will allow the stainless steel to function as a cathode in the coupling with carbon steel leading to bimetallic corrosion of the second. The corrosion rate of carbon steel where CO_2 is present throughout the system (at both material surfaces) is 0.384 mm/y at 23°C, similar to that of carbon steel coupled to lead in deareated CO_2-free brine at 70 °C (0.139 and 0.383 mm/y at 25° and 70° C respectively). Both magnitudes higher than the corrosion rate of carbon steel on its own in deaerated geothermal brine (0.058 mm/y at 25° C). This underlines that degassing or controlling the solubility of CO_2 in the system is important, although the effect of temperature has not been investigated in the specific case of CO_2 induced galvanic corrosion. With the high conductivity and thus large areas affected by galvanic couplings, the influence of area sizes will, as always, play a role in the corrosive effect of the galvanic coupling. Noteworthy is how the corrosion rate of carbon steel is also high (0.283 mm/y) in the case where it may be separated from the CO_2 containing brine via a membrane. The observed anodic polarisation may also interfere with the efficacy of corrosion inhibitors, added to protect the carbon steel. Thus, in areas where there is there kind of connections and increased corrosion rate of the carbon steel can be expected. However, it must be mentioned that the CO_2 studies carried out in this study is done with purging with pure CO_2 when the gas is used, and thus the effect of gas composition and concentration along with its effect on chemical balances in the brine and corrosiveness has not been investigated.

The main conclusions of the individual test series are summarised below:

- Monitor changes in dissolved oxygen and pH during operation of geothermal plants
  - pH is very stable with only minor variation
  - Dissolved oxygen (DO) is below the detection limit, i.e. in the ppb range
  - During operating excursions, e.g. shutdown procedure, DO has been observed to go as high as in the 100 ppb range

- Study effects of lead and copper deposition on corrosion of steel, including effects of temperature, concentration and galvanic coupling
  - Tafel extrapolation from potentiodynamic polarisation
    - Show a corrosion rate of 0.023 mm/y for carbon steel in pure artificial Margretheholm brine. Without Pb(II) in solution, the effect of temperature (25 vs 70 °C) is absent
    - Temperature (25 vs 70 °C) did not show a clear effect on the corrosion rate of carbon steel with 3.0 mg/l Pb(II)

        - With increased Pb(II) content (22.5 mg/l) a clear effect of temperature is seen – 0.06 and 0.11 mm/y for 25 and 70 °C respectively
    - Evans diagrams – based on individual potentiodynamic polarisations
        - The coupling between carbon steel and already deposited lead give a moderate increase to carbon steels corrosion rate with 0.047 mm/y. No clear effect of temperature observed.
        - Coupling between carbon steel and lead, where 3.0 mg/l Pb(II) is present in solution show a large increase in corrosion rate and large increase with increasing temperature – corrosion rate of 0.139 and 0.383 mm/y for 25 and 70 °C respectively
    - Zero resistance amperometry
        - Physically creating the coupling of carbon steel and carbon steel where 3.0 mg/l Pb(II) is found in solution show that there is in fact an influence of temperature on the deposition kinetics and corrosion rate with 0.012 and 0.029 mm/y at 25 and 70 °C respectively
        - Increase in Pb(II) concentration (from 3.0 to 22.5 mg/l) gave rise to an increase in corrosion rate of carbon steel measuring 0.024 mm/y at 23 °C

- Corrosion inhibitors
    - Tafel extrapolation
        - Show more than a factor 5 reduction in corrosion rate with both 1 and 10 ppm Nalco GEO942 added in the brine without Pb(II) at 25 °C, while also showing a rise in corrosion potential
        - Increase from 1 to 10 ppm at 70 °C show an unwanted effect of increased corrosion rate (0.01 mm/y from 0.004 mm/y) possibly due to the 100 mV increase in corrosion potential polarising the steel where the inhibitor has not yet formed a protective film
    - Linear polarisation resistance
        - Show a similar corrosion rate with 0.01 mm/y with only 1 ppm inhibitor, indicating variations in inhibitor effect are common
        - With 3.0 mg/l Pb(II) and 1 ppm inhibitor it is evident that time is an important factor in the efficiency of the inhibitor – reduction from 0.014 to 0.005 mm/y after 3 hours
        - Access to the sample surface also play a key role as shown by stagnant condition leading to higher corrosion rates

- Calculate extension of galvanic element by lead as function of chloride/conductivity
    - The differences in corrosion behaviour observed in the PCA cannot entirely be explained by increased chloride content leading to increased conductivity. This is shown by mathematic modelling of corrosion rate and extension of galvanic elements in geothermal brine. Thus, other mechanisms are suspected to interact, i.e. complexing of chloride with either lead or iron

- Study effects of lead and copper deposition on corrosion behaviour or CRAs
    - Lead was electrochemically less noble than both CRAs and thus no galvanic driving force for the deposition of lead onto the surface of these steels
    - It is evident that AISI 316L exhibits a behaviour indicative of borderline compatibility in the brine
    - L80-13Cr is unsuitable for use in the geothermal brine

- Study effect of dissolved oxygen on corrosion resistance of CRAs
    - Oxygen ingress does not show a significant effect on neither open circuit potential nor on pitting potential of AISI 316L
    - The effect of DO on platinum show surface potential increases capable of initiating corrosion of AISI 316L

- The behaviour of AISI 316L with increasing DO underlines its borderline compatibility and the low repassivation potential shows that once corrosion has initiated it may not stop again

- Study influence of CO_2 on galvanic corrosion
  - Presence of CO_2 will allow the stainless steel to function as a cathode in the coupling with carbon steel leading to bimetallic corrosion of the latter
  - CO_2 presence throughout the system gave a corrosion rate of 0.384 mm/y at 23°C
  - The corrosion rate for carbon steel alone, calculated using NORSOK M-506, is 4.2 mm/year under the same conditions (pH 3.77, 1 bar CO_2). Thus, the corrosion contribution from the galvanic coupling to the more noble AISI 316L give only a moderate increase of 9 % increase

5 References and literature

1. Anastasia Stoljarova, Masterarbeit, Effect of Lead On Steel Corrosion in Geothermal Systems Institut Für Chemie Und Biochemie, Freie Universität Berlin, 10. September 2019
2. Anastasia Stoljarova, Simona Regenspurg, Ralph Bäßler, Troels Mathiesen, Johan Braüner Nielsen; Effect of lead- and copper containing brine on steel materials for geothermal applications – a corrosion study. Geothermics 91: 102024, 2020.
3. H. Schröder et al, Long term reliability of geothermal plants – Examples from Germany, Proceedings European Geothermal Congress 2007, Unterhaching, Germany, 30 May-1 June 2007.
4. Lead in formation water causes problems in geothermal exploitation, GEUS rapport, 15-10-2015.
5. Nye undersøgelser indikerer at partikelindholdet i injektionsvandet øges når køling ikke fungerer, GEUS rapport, 16-02-2015.
6. Partikler i injektionsvand i injektionsvand membran filterprøver udtaget 16. februar 2015 på GDA, GEUS rapport, 16-02-2015.
7. Partikler i injektionsvand membran filterprøver udtaget 14. januar 2015 på GDA, GEUS rapport, 14-01-2015.
8. Troels Mathiesen, Jakob Mølholm og Johan Braüner Nielsen, Results of on-site monitoring campaign and parametric laboratory testing Results of on-site monitoring campaign and parametric laboratory testing, GEOTHERM project 6154-00011B, 2019.
9. Thisted suspended solids and formation water chemistry December 2015, GEUS notat, 27-04-2016.
10. Metals Handbook, 9th edition, Volume 13 – Corrosion, Corrosion of Lead and Lead Alloys, 1987.
11. H. Osvoll and JC Werenskiold, CP design of internal components, EuroCorr2014, Paper 7747.
12. NORSOK STANDARD M-001 Rev. 3, Nov. 2002
13. NORSOK M-506:2017, CO2 corrosion rate calculation.

Appendix

Copy of Journal article – only for distribution within project group due to copyrights.

Anastasia Stoljarova, Simona Regenspurg, Ralph Bäßler, Troels Mathiesen, Johan Braüner Nielsen; Effect of lead- and copper containing brine on steel materials for geothermal applications – a corrosion study. Geothermics 91: 102024, 2020.